Discrete Time Quantum Walk in a QCD Chiral Condensate Lattice

Rami Rom *

Posted Date: 14 April 2026

doi: 10.20944/preprints202604.0893.v1

Keywords: Baryon separation; QCD condensate; Pmmm space group; instanton liquid; discrete time quantum walk (DTQW); antimatter; black holes (BH); Cooper pairs

 doi:10.20944/preprints202604.0893.v1

Article

Discrete Time Quantum Walk in a QCD Chiral Condensate Lattice

Rami Rom

Independent Researcher; rami@rom-ip-service.com; Tel.: +972-50-886-7433

Abstract

We propose a chiral condensate lattice with Pmmm space group symmetry (No. 47, D2h, order 8) and a cubic unit cell built from the four light quarks and antiquarks, $\tilde{u}u\tilde{d}d$, hypothesized to serve as the fundamental building blocks of the chiral condensate lattice and of baryonic and leptonic matter. The proposed Pmmm chiral condensate lattice arises from spontaneous symmetry breaking of the parent $Pm\bar{3}m$ space group (No. 221, Oh, order 48), with the 40 broken symmetry operations generating the three pions π^+, π^-, π^0 as Goldstone bosons, and is proposed as an alternative structural description of the instanton liquid QCD chiral condensate. Electrons and positrons are embedded within the chiral condensate lattice and perform discrete-time quantum walks (DTQW) driven by underlying quark and antiquark permutations between the highly symmetric Wyckoff positions of the Pmmm unit cell, analogous to quark hopping in the instanton liquid. We assume that quark permutations occur at the Zitterbewegung frequency, ensuring that the embedded electron is never bare and generating a confined electron cloud within the chiral condensate lattice. The spin and helicity states of the embedded electrons are structurally defined by the chiral condensate structure and dynamics: the quantum walker type, matter or antimatter, determines the spin state, while the helicity state depends on whether the motion of the larger quark charge is parallel or antiparallel to the motion of the embedded electron charge. We assume that an electron undergoing a DTQW embedded within the chiral condensate lattice produces a coherent wave packet, in contrast to the wave packet dispersion found by Schrödinger and Darwin in 1927, which may provide indirect evidence for the existence of the proposed Pmmm chiral condensate lattice. A one-dimensional DTQW simulation with a non-Hermitian quantum coin generates coherent evolution of one wave packet component, providing promising support for the proposed framework. We further assume that in the vicinity of black hole horizons the chiral condensate lattice melts, thereby enabling a reaction of three Pionic tetraquarks that produce deuteron and anti-deuteron pairs, which further react with Pionic tetraquarks to produce protons, electrons, and anti-neutrons that fall beneath the black hole horizon while matter particles escape.

Keywords: Baryon separation; QCD condensate; Pmmm space group; instanton liquid; discrete time quantum walk (DTQW); antimatter; black holes (BH); Cooper pairs

1. Introduction

Which process broke the symmetry between matter and antimatter? In "Baryon Asymmetry, Dark Matter and Quantum Chromodynamics", Oaknin and Zhitnitsky [1] proposed an innovative explanation rooted in nonperturbative quantum chromodynamics (QCD). Their scenario suggests that at the end of the cosmological QCD phase transition, quarks and antiquarks separated into two distinct phases: ordinary hadrons (and antihadrons), as well as massive lumps (and antilumps) of a novel color superconducting phase that may serve as cosmological cold dark matter. We propose herein below an alternative process for matter–antimatter separation based on pion tetraquark reactions enabled by the melting of the QCD chiral condensate lattice [2–6] near black hole horizons.

The chiral condensate is described as interacting instanton and anti-instanton liquid [7] with an estimated density of one instanton in a fermi cube. According to the instanton liquid theory, the

 doi:10.20944/preprints202604.0893.v1

ground state of QCD is a dense state, composed of gauge fields and quarks. The instantons act as potential wells, in which light quarks can form bound states. Quarks can travel over large distances by hopping from one instanton to another similar to electron motion in a conductor. The chiral condensate is related to Dirac operator density of states near zero energy by the Banks-Casher relation [8], which can be related to the zero energy states of the quarks bound states in the instanton liquid potential wells.

We propose herein below that like in the interacting instanton liquid theory, the four light quarks and antiquarks, $u, \tilde{u}, d, \tilde{d}$, that generate the unit cell of the Pmmm space group chiral condensate lattice shown in FIG. 2a below, can walk in the chiral condensate lattice by tunnelling and permutations between specific allowed Pmmm lattice sites high symmetry Wyckoff positions and can provide the zero energy states for the Banks-Casher relation. We further propose that in the vicinity of black hole horizons the chiral condensate lattice melts, thereby enabling reactions of three pion tetraquarks that produce deuteron and anti-deuteron pairs [39] that further react with pion tetraquarks producing protons, electrons and anti-neutrons that fall beneath the BH horizon while the matter particles escape.

Erwin Schrödinger introduced the concept of a wave packet particle and found that a Gaussian wave packet remains coherent within a harmonic potential. However, Schrödinger and Darwin discovered that in empty space, the particle wave packet disperse where the width of a Gaussian wave packet grows rapidly with time [9]. If an electron wave packet is initially localized in a region of atomic dimensions (10^{-10} meter), the width of the wave packet doubles in approximately 10^{-16} second, and after about a millisecond, the wave packet width expands to roughly a kilometer, an unreasonable result for a point-like particle [10]. This raises fundamental questions: Is the Schrödinger equation invalid for free electrons, or alternatively, is our understanding of empty space incorrect, as Dirac suggested in his lecture on electrons and the vacuum [11]. If the latter is true, can the discrete-time quantum walk (DTQW) framework [12] produce coherent wave packet evolution in the proposed chiral condensate lattice?

Unlike classical random walks, where a coin flip determines the direction of each step, quantum walks use "quantum coins" such as the quantum walker's spin or polarization, allowing quantum superposition and interference to occur. In one dimension, this enables simultaneous movement of the quantum walker in both directions, resulting in faster, linear propagation compared to the square-root scaling of classical random walks [13]. DTQWs can be used to implement universal quantum gate sets for quantum computation [14]. Additionally, DTQWs are utilized to study the dynamics of various topological phases, each defined by topological invariants that reflect the global structure of their ground state wavefunctions. In a DTQW, a walker possessing a two-level internal spin moves between neighboring lattice sites through a sequence of unitary operations. The DTQW protocol can be tailored to satisfy criteria such as time-reversal and particle-hole symmetries [15]. Two-dimensional DTQWs have been employed to protect Bell-state entanglement in a single photon by using edge states at the interface of different quantum walk domains [16]. Continuous quantum walks of photons in waveguide lattices have been found to exhibit ballistic propagation in the free dimension along the waveguides [17]. Quantum walks of interacting electrons have been demonstrated using semiconductor quantum dots arranged in a circular configuration, where a single electron occupies a quantum dot and can encode a qubit. Electrons perform a continuous quantum walk (CQW) by tunneling through a barrier of controlled applied voltage between the quantum dots in circle [18]. DTQW methods have been applied to simulate QCD parton showers on quantum computers, where emission probabilities act as the coin flip, and parton emissions, either gluons or quark pairs, are represented by the quantum walker's movement in two dimensions [19]. It should be noted that parton shower quantum walks stem from extremely high-energy collisions, whereas this paper focuses on the ground-state dynamics of the chiral condensate and the behavior of embedded electrons as they walk and tunnel between lattice sites via rapid quark permutations at low temperatures.

 doi:10.20944/preprints202604.0893.v1

This paper proposes a framework that goes beyond the Standard Model by introducing a Pmmm space group unit cell for the non-empty vacuum of Quantum Field Theory (QFT), upon which Quantum Chromodynamics (QCD) relies, while addressing the longstanding absence of a structural description for the non-zero vacuum expectation value (VEV) of the QCD Pionic condensate. An alternative model for matter–antimatter separation is proposed in Section 2. Section 3 explores quark discrete-time quantum walks within the chiral condensate lattice and examines quark topological phases. The chiral condensate lattice and the Pmmm space group are described in Section 4. Section 5 addresses the DTQWs of embedded electrons and positrons within the chiral condensate based on the Pmmm space group symmetric allowed quark permutations, while Section 6 focuses on the characteristics of embedded Cooper pairs. Processes involving electron-positron creation and annihilation within the chiral condensate are examined in Section 7. Pmmm ionic lattice analog of the QCD chiral condensate lattice is described in Section 8. One-dimension DTQW simulations are presented in Section 9. Finally, Section 10 is a discussion. Appendix A describes the derivation of the chiral condensate lattice tight-binding hopping Hamiltonian model.

2. The Question of Matter and Antimatter Separation

In this work, we propose an alternative separation model that could create the matter–antimatter asymmetry using balanced quark reaction equations. Our model suggests that antimatter is hidden from the observable universe beneath black hole horizons, effectively separating it from ordinary matter. We further assume that regions near black hole horizons contain extremely hot and dense pion tetraquark liquid, $\tilde{u}\,u\tilde{d}d$, due to local melting of the QCD chiral condensate lattice [20]. The tetraquark boson density, $\tilde{u}\,u\tilde{d}d$, can be greatly amplified by the black hole laser effect within the BH ergosphere [21].

Three pion tetraquarks from the melted chiral condensate may react creating a deuteron and antideuteron according to Eq. 1. The extremely high density of pion tetraquarks react with the products of Eq. 1, whereby neutrons are converted to protons and antiprotons are converted to antineutrons according to Eqs. 2 and 3. Two antineutrons fall beneath the BH event horizon, becoming invisible, while two protons and two negatively charged tetraquarks, which may be composite electrons, escape into space via Hawking radiation [22]. The overall balanced reaction is summarized in Eq. 4.

$$3\ \tilde{u}\,u\tilde{d}d \rightarrow\ uddduud\ +\ \tilde{u}\tilde{d}\,\tilde{d}\,\tilde{u}\tilde{u}\tilde{d} \tag{1}$$

$$udd\ +\ \tilde{u}\,u\tilde{d}d \rightarrow\ uud +\ d\tilde{d}d\tilde{u} \tag{2}$$

$$\tilde{u}\tilde{u}\tilde{d}\ +\ \tilde{u}\,u\tilde{d}d \rightarrow\ \tilde{u}\tilde{d}\tilde{d}\ +\ \tilde{u}\,u\tilde{u}d \tag{3}$$

$$5\ \tilde{u}\,u\tilde{d}d \rightarrow 2\ \tilde{u}\tilde{d}\tilde{d}\ +\ 2\,uud + d\tilde{d}d\tilde{u} +\ \tilde{u}\,ud\tilde{u} \tag{4}$$

Equations 2 and 3 represent second-order β-decay-like reactions in which neutrons and antiprotons react with pion tetraquarks to produce protons and antineutrons, respectively. These reactions are triggered by collisions with pion tetraquarks in the vicinity of black hole horizons and conserve quark and antiquark equilibrium without quark creation or annihilation. Accordingly, near black hole horizons, matter–antimatter symmetry is broken as pion tetraquarks react to form matter–antimatter pairs: antimatter falls into the black hole, whereas matter particles escape. Furthermore, the β-decay-like second-order reaction kinetics described in Eqs. 2 and 3 suggest that electrons may be composite particles consisting of quarks and antiquarks, potentially existing in two distinct forms $\tilde{u}d\tilde{d}\,d$ and $\tilde{u}d\tilde{u}\,u$.

Quark reaction equations 1–4 provide an alternative model for matter-antimatter symmetry breaking near black holes, which may continuously create matter [23]. In Section 3, we propose that pion tetraquarks condense into a lattice, forming the chiral condensate lattice with a Pmmm space

 doi:10.20944/preprints202604.0893.v1

group cubic unit cell illustrated in Figure 2a-b. We propose that quarks and antiquarks perform quantum walks within the chiral condensate lattice.

It should be noted that the formation of deuteron and anti-deuteron pairs from three-pion tetraquarks in the vicinity of black hole horizons according to Eq. 1 is non-trivial. Recently, the ALICE Collaboration published a paper addressing deuteron and anti-deuteron formation and proposed a novel approach using deuteron–pion momentum correlations in proton-proton (pp) collisions at the Large Hadron Collider (LHC) [39]. The temperature of the proton-proton collisions at the LHC may be similar to the temperature in accretion disks in the vicinity of black hole horizons and may locally melt the chiral condensate lattice, thereby enabling the reaction of three-pion tetraquarks to produce deuteron and anti-deuteron pairs according to Eq. 1

3. Discrete-Time Quantum Walk in the Pionic Fabric

We assume that $u, d, \tilde{u}, \tilde{d}$ quarks and antiquarks are the basic elements of the QCD vacuum, forming the chiral condensate lattice [24] and serving as fundamental components of both baryonic and leptonic matter, as suggested by Harari's four sub-particles model $T, V, \tilde{T}, \tilde{V}$ [25]. The chiral condensate sub-unit cubic cell consists of two rotated pion tetraquark tetrahedrons shown in Figures 1a and 1b.

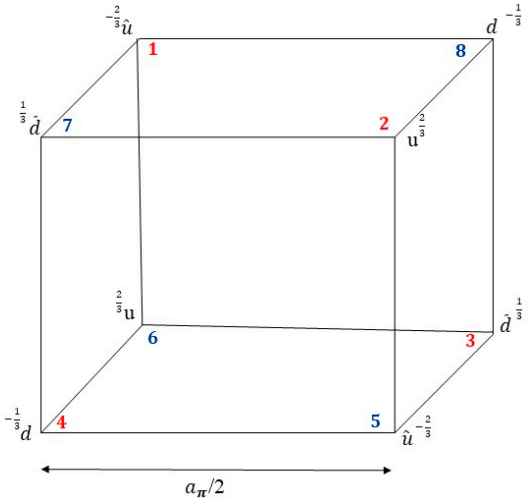

FIG. 1a illustrates the chiral condensate proposed sub-unit cell

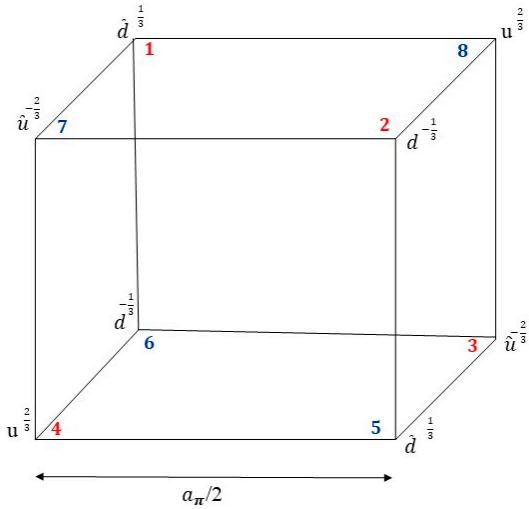

FIG. 1b illustrates the chiral condensate proposed sub-unit cell enantiomer

Preprints.org (www.preprints.org) | NOT PEER-REVIEWED | Posted: 14 April 2026 doi:10.20944/preprints202604.0893.v1

Eight quarks and antiquarks occupy the sub-unit cell corners, with combined chargeless, colorless pions $\tilde{u}\,u\,d\,\tilde{d}$ positioned on each face of the cube. The two tetraquark molecules are labeled by indices (1–4) and (5–8), allowing the definition of an eight-component spinor and permutation matrices. Since the sub-unit cell contains equal numbers of quarks and antiquarks, the QCD chiral condensate lattice that fills empty space is not composed of regular matter. The complete Pmmm space group chiral condensate cubic unit cell is illustrated in Figure 2a-b. The quark and antiquark highly symmetric Wyckoff positions in the Pmmm space group of length a are: d: (0,0,0) (a,0,0) (0,a,0) (0,0,a) (0,a,a) (a,a,0) (a,0,a) (a,a,a) (a/2,a/2,a/2); $\tilde{d}$: (0,0,a/2) (a,0,a/2) (0,a,a/2) (a,a,a/2) (a/2,a/2,0) (a/2,a/2,a); u: (0,a/2,0) (a,a/2,0) (0,a/2,a) (a,a/2,a) (a/2,0,a/2) (a/2,a,a/2); and $\tilde{u}$: (a/2,0,0) (a/2,a,0) (a/2,0,a) (a/2,a,a) (0,a/2,a/2) (a,a/2,a/2). For clarity, the sub-unit cell shown in Figure 1a is highlighted in red in Figure 2a and 2b below.

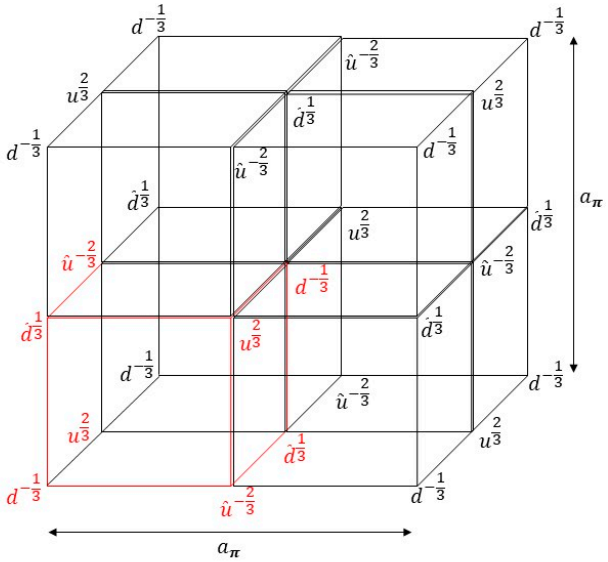

FIG. 2a illustrates the chiral condensate proposed unit cell

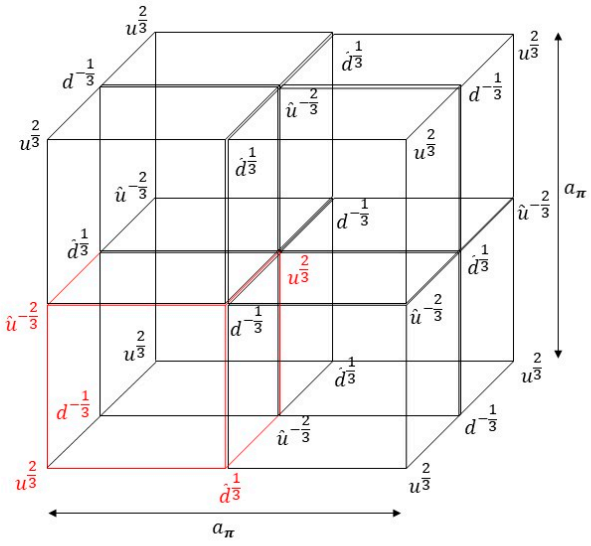

FIG. 2b illustrates the chiral condensate proposed unit cell with a π phase change

The chiral condensate lattice unit cell has a Pmmm space group #47 with D_{2h} point group symmetry which is a sub-group of the $Pm\bar{3}m$ space group #221 that has the full O_h symmetry as described in more details in Section 4 below.

 doi:10.20944/preprints202604.0893.v1

We propose that embedded electrons, quarks, and antiquarks perform discrete-time quantum walks (DTQW) [12–19] in the QCD chiral condensate lattice by tunneling between highly symmetric Pmmm space group Wyckoff lattice sites by rapid permutations. In the DTQW context, the quantum coin, the quantum hidden variable of the quantum walker, could be the quark's flavor, type (matter or antimatter) and the symmetric Wyckoff positions in the unit cell. As described below in Section 4, selection rules are enforced that allow hopping of quarks-to-quarks positions only, d and u hoping, and antiquarks-to-antiquarks position only $\tilde{d}$ and $\tilde{u}$, between lattice sites determined by the Pmmm space group. The chiral condensate wavefunction and the quantum walk within the chiral condensate lattice may be represented by spinors and permutation matrices, as described in subsequent sections. The chiral condensate lattice permutation matrices generalize the Conditional-NOT (C-NOT) two-qubit quantum gate, given, for example, by the four-by-four matrix in Equation 8 (page 4) of "Universal quantum computation using the discrete time quantum walk" [14].

$$C_{NOT} = \begin{bmatrix} 1 & 0 & 0 & 0 \\ 0 & 1 & 0 & 0 \\ 0 & 0 & 0 & 1 \\ 0 & 0 & 1 & 0 \end{bmatrix} \quad \text{Eq. 4}$$

The permutation matrix in Equation 5 swaps quarks and antiquarks between corners of the sub-cubic unit cell shown in Figure 1a, transforming it into its enantiomer mirror cell depicted in Figure 1b.

$$\begin{bmatrix} \psi_{\tilde{d}}(1) \\ \psi_{d}(2) \\ \psi_{\tilde{u}}(3) \\ \psi_{u}(4) \\ \psi_{\tilde{d}}(5) \\ \psi_{d}(6) \\ \psi_{\tilde{u}}(7) \\ \psi_{u}(8) \end{bmatrix} = \begin{bmatrix} 0 & 0 & 0 & 0 & 0 & 0 & 1 & 0 \\ 0 & 0 & 0 & 0 & 0 & 0 & 0 & 1 \\ 0 & 0 & 0 & 0 & 1 & 0 & 0 & 0 \\ 0 & 0 & 0 & 0 & 0 & 1 & 0 & 0 \\ 0 & 0 & 1 & 0 & 0 & 0 & 0 & 0 \\ 0 & 0 & 0 & 1 & 0 & 0 & 0 & 0 \\ 1 & 0 & 0 & 0 & 0 & 0 & 0 & 0 \\ 0 & 1 & 0 & 0 & 0 & 0 & 0 & 0 \end{bmatrix} \begin{bmatrix} \psi_{\tilde{u}}(1) \\ \psi_{u}(2) \\ \psi_{\tilde{d}}(3) \\ \psi_{d}(4) \\ \psi_{\tilde{u}}(5) \\ \psi_{u}(6) \\ \psi_{\tilde{d}}(7) \\ \psi_{d}(8) \end{bmatrix} \quad \text{Eq. 5}$$

We note that the Pmmm space group electrically neutral chiral condensate lattice unit cell can be charged by replacing a single quark or antiquark embedding a charged electron or positron, as illustrated in Section 5. With the embedded electron or positron, the underlying quark and antiquark permutation matrices describe the embedded electron's or positron's DTQW, which differs from both Bohr's hydrogen atom classical electron trajectories and Heisenberg's quantum theory [26], and also from the free electron solution of the Schrödinger equation [9,10]. Additionally, while the chiral condensate lattice cubic unit cell characterizes the flat empty space, we propose that proximity to a massive or charged body causes the chiral condensate lattice unit cell to reshape, becoming more compact and curved, potentially representing the microscopic origin of the curved spacetime of general relativity [27].

4. The Chiral Condensate Lattice and the Pmmm Space Group

The proposed chiral condensate lattice illustrated in Figure 2a, has a parent cubic $Pm\bar{3}m$ space group symmetry broken to a Pmmm space group unit cell. We assume that upon condensation of the chiral condensate lattice, the four-light quark $\tilde{u}\, u\, d\, \tilde{d}$ occupy the Pmmm highly symmetric Wyckoff positions shown in Figure 2a, breaking the symmetry from $Pm\bar{3}m$ O_h order 48 symmetry to Pmmm D_{2h} order 8 space group. The 40 broken symmetry operations may be the geometric analog for the generation of QCD's Goldstone boson spectrum, with the three broken rotational directions corresponding to QCD's three pions π^+, π^-, π^0. The Pmmm space group symmetry preserves inversion, three mirror planes, and three two-fold axes, consistent with the conserved isospin and parity of QCD vacuum.

 doi:10.20944/preprints202604.0893.v1

A tight-binding hopping Hamiltonian model for the Pmmm space group unit cell is constructed below following the tight-binding second quantization formalism developed for multi-site cubic perovskite structures [29,40], with Wyckoff site assignments and symmetry-allowed hopping integrals determined by the D2h point group of Pmmm space group No. 47. Enforcing the hopping amplitudes to only quarks and quarks swapping and antiquarks and antiquarks swapping, d and u hoping or $\tilde{d}$ and $\tilde{u}$ hopping, decouples the tight binding hopping Hamiltonian to quarks and antiquarks 4 by 4 block sectors. The tight-binding hopping Hamiltonian model in Fourier k-space is symmetric and analytically solvable as shown in the Appendix.

$$H(\vec{k}) = \begin{vmatrix} \mathcal{E}_d & 0 & 4t_{du}cx\,cz & 2t_{du}\mathrm{cy} & & & & \\ 0 & \mathcal{E}_d & 2t_{du}\mathrm{cy} & 4t_{du}cx\,cz & & & & \\ 4t_{du}cx\,cz & 2t_{du}\mathrm{cy} & \mathcal{E}_u & 0 & & & & \\ 2t_{du}\mathrm{cy} & 4t_{du}cx\,cz & 0 & \mathcal{E}_u & & & & \\ & & & & 0 & 0 & 0 & 0 \\ & & & & 0 & 0 & 0 & 0 \\ & & & & 0 & 0 & 0 & 0 \\ & & & & 0 & 0 & 0 & 0 \\ & & & & & & & \\ & & & & \mathcal{E}_{\tilde{d}} & 0 & 4t_{\tilde{d}\tilde{u}}cx\,cy & 2t_{\tilde{d}\tilde{u}}\mathrm{cz} \\ & & & & 0 & \mathcal{E}_{\tilde{d}} & 2t_{\tilde{d}\tilde{u}}\mathrm{cz} & 4t_{\tilde{d}\tilde{u}}cx\,cy \\ & & & & 4t_{\tilde{d}\tilde{u}}cx\,cy & 2t_{\tilde{d}\tilde{u}}\mathrm{cz} & \mathcal{E}_{\tilde{u}} & 0 \\ & & & & 2t_{\tilde{d}\tilde{u}}\mathrm{cz} & 4t_{\tilde{d}\tilde{u}}cx\,cy & 0 & \mathcal{E}_{\tilde{u}} \end{vmatrix} \quad \text{Eq. 6a}$$

where $\mathrm{cx} = \cos(0.5k_x a)$, $\mathrm{cy} = \cos(0.5k_y a)$ and $\mathrm{cz} = \cos(0.5k_z a)$ and the six parameters of the tight-binding hopping Hamiltonian model are the quark and antiquark energies, $\mathcal{E}_d, \mathcal{E}_u, \mathcal{E}_{\tilde{d}}, \mathcal{E}_{\tilde{u}}$ and the symmetry allowed hopping amplitudes t_{du} and $t_{\tilde{d}\tilde{u}}$. The two 4 by 4 decoupled Hamiltonian blocks allow analytical solutions for tt$_{du}$he eight energy bands.

$$E_{1,2} = \frac{\mathcal{E}_d+\mathcal{E}_u}{2} \pm \sqrt{\left(\frac{\mathcal{E}_d-\mathcal{E}_u}{2}\right)^2 + (2t_{du})^2(2\,cx\,cz + cy)^2} \quad \text{Eq. 6b}$$

$$E_{3,4} = \frac{\mathcal{E}_d+\mathcal{E}_u}{2} \pm \sqrt{\left(\frac{\mathcal{E}_d-\mathcal{E}_u}{2}\right)^2 + (2t_{du})^2(2\,cx\,cz - cy)^2} \quad \text{Eq. 6c}$$

$$E_{5,6} = \frac{\mathcal{E}_{\tilde{d}}+\mathcal{E}_{\tilde{u}}}{2} \pm \sqrt{\left(\frac{\mathcal{E}_{\tilde{d}}-\mathcal{E}_{\tilde{u}}}{2}\right)^2 + (2t_{\tilde{d}\tilde{u}})^2(2\,cx\,cy + cz)^2} \quad \text{Eq. 6d}$$

$$E_{7,8} = \frac{\mathcal{E}_{\tilde{d}}+\mathcal{E}_{\tilde{u}}}{2} \pm \sqrt{\left(\frac{\mathcal{E}_{\tilde{d}}-\mathcal{E}_{\tilde{u}}}{2}\right)^2 + (2t_{\tilde{d}\tilde{u}})^2(2\,cx\,cy - cz)^2} \quad \text{Eq. 6e}$$

The enforced selection rules are in line with the proposed embedded electron dynamics in the chiral condensate lattice model described in Section 5. The d and u hopping decoupled from the $\tilde{d}$ and $\tilde{u}$ hopping produce two types of embedded electron dynamics in the chiral condensate lattice, motion of quarks is decoupled from morion of antiquarks as seen also with the Hamiltonian's energy band solution. The tight binding hopping block-diagonal Hamiltonian and energy bands support the proposed model of the chiral condensate lattice Pmmm space group unit cell. The derivation of the chiral condensate lattice tight-binding hopping Hamiltonian model is described in the Appendix.

A central gap in the Standard Model (SM) is the absence of a structural account for the non-zero vacuum expectation value of the QCD Pionic condensate. The chiral condensate order parameter arises in the proposed Pmmm chiral condensate lattice as the coherent overlap between the d quark wavefunction at Wyckoff sites 1a and 1b and the u quark wavefunction at the 3c-type sites, mediated by the hopping amplitude t_{du}. The non-zero VEV is therefore a structural property of the proposed Pmmm space group.

In the chiral limit, $\mathcal{E}_d = \mathcal{E}_u$ and $\mathcal{E}_{\tilde{d}} = \mathcal{E}_{\tilde{u}}$, the band gap between the symmetric and antisymmetric quark bands at the Γ point, k= (0,0,0), equals $4t_{du}$, which may serve as the chiral condensate lattice analog of the pion mass m_π. The chiral condensate lattice VEV is proportional to the hopping amplitude $4t_{du}$. When $t_{du} \neq 0$, d and u quarks mix through hopping, generating a non-zero ground state overlap, the VEV is non-zero in the ground state due to tunneling between the symmetric Wyckoff positions. The Pmmm space group, obtained by symmetry breaking from the Pm3¯m space group, provides a consistent, geometrically grounded description of the QCD non-empty vacuum. The non-zero VEV of the QCD Pionic condensate, which lacks a description within the Standard Model framework, emerges in the proposed chiral condensate lattice as a geometric asymmetry of the Pmmm unit cell, specifically, the inequivalent treatment of the three spatial directions occupied by the $\tilde{u}, u, \tilde{d}$ quark species after condensation (where d occupy the (0,0,0) Wyckoff position). The proposed chiral lattice model provides the missing geometric scaffolding

 doi:10.20944/preprints202604.0893.v1

upon which the QCD vacuum structure is built, offering a crystallographic description of the non-empty QCD vacuum consistent with chiral symmetry breaking.

5. Embedded Electrons and Positrons Confinement Clouds and Quark DTQW in the Pmmm Chiral Condensate Lattice

If neutron β-decay kinetics is modeled as a second-order reaction triggered by collision with a Pionic tetraquark [31], the result is a positively charged proton and a negatively charged exotic tetraquark, which may serve as an embedded electron within the chiral condensate, as shown in Equation 7.

$$udd(N) + \tilde{u}d\tilde{d}u\,(\pi^0) \rightarrow udu(P^+) + \tilde{u}d\tilde{d}d\,(e^-)\; Eq.(7)$$

The balanced reaction equation maintains both quark number and flavor, linking embedded electrons to pion tetraquarks, these can interconvert through adjacent quark permutations within the chiral condensate. Shifting between a pion tetraquark $\tilde{u}d\tilde{d}u$ and an electron tetraquark $\tilde{u}d\tilde{d}d$ requires swapping a u quark with a d quark. Note that in addition to Harari's schematic model of quarks and leptons composite particles [25]. Davidson suggested recently that leptons are made of three pre-leptons with fractional charges at the fundamental level [37]. The pion and electron tetraquarks symmetric quark exchange reaction between Pionic fabric sites is described in Eq. (8) where the d and the u quarks are swapped. Since the reactants and products are identical a double well potential model may be used to describe the quark exchange reaction that can occur by quantum tunnelling through a potential barrier similar to ammonia molecule inversion [30].

$$\tilde{u}d\tilde{d}d\,(e^-) + \tilde{u}d\tilde{d}u\,(\pi^0) \rightarrow \tilde{u}d\tilde{d}u\,(\pi^0) + \tilde{u}d\tilde{d}d\,(e^-)\; Eq.(8)$$

According to the assumed chiral lattice Pmmm unit cell symmetry, $\tilde{u}$ and $\tilde{d}$ antiquarks may be similarly swapped according to the Eq. (9).

$$\tilde{u}d\tilde{u}u\,(e^-) + \tilde{u}d\tilde{d}u\,(\pi^0) \rightarrow \tilde{u}d\tilde{d}u\,(\pi^0) + \tilde{u}d\tilde{u}u\,(e^-)\; Eq.(9)$$

The symmetric d and u and $\tilde{u}$ and $\tilde{d}$ quark exchange reactions between embedded electron tetraquark and pion tetraquark in the chiral lattice may be seen as a hidden internal symmetry that according to the SM generates charge and current conservation [1]. The electric charge and current are carried by the d and u quark swapping according to Equation (8) and $\tilde{u}$ and $\tilde{d}$ antiquark exchanges according to Equation (9) in the proposed chiral lattice.

It should be noted that in deuterium nucleus, a similar quark exchange reaction may occur, exchanging d and u quarks between the proton and neutron, as shown in Eq. 10.

$$udd(N) + udu(P^+) \rightarrow udu(P^+) + udd(N)\; Eq.(10)$$

Since the proposed chiral condensate lattice is built from Pionic tetraquarks, rapid quark permutations between composite electron tetraquarks and neighboring Pionic tetraquarks in adjacent unit cells of the chiral condensate lattice can occur. Consequently, an embedded electron cloud may form within the chiral lattice. These rapid quark permutation reactions make it impossible to determine the exact location of the composite embedded electron, a result consistent with quantum mechanics and Heisenberg uncertainty principle.

Embedded electrons and positrons can be produced within the proposed Pmmm space group chiral condensate unit cell by replacing a quark or antiquark in specific high symmetry Wyckoff positions as outlined in the following examples. The Pmmm chiral condensate lattice with the enforced hopping selection rules allows two types of embedded electron and positron configurations. Figure 3 depicts a type I embedded electron cell, formed by replacing a d quark with a u quark at Wyckoff site (a/2, 0, a/2) of the unit cell. Hence the unit cell carries a -1 electric charge. Two green arrows in Figure 3 indicate symmetry allowed quantum walk hopping of the substituted d quark inside the unit cell to Wyckoff positions (0, a/2, 0) and (a, a/2, 0).

Preprints.org (www.preprints.org) | NOT PEER-REVIEWED | Posted: 14 April 2026 doi:10.20944/preprints202604.0893.v1

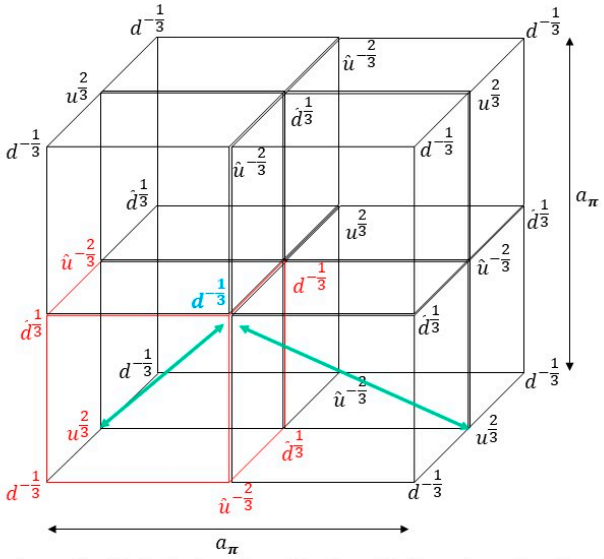

Figure 3 illustrates embedded electron type I in the chiral condensate where two possible permutations out of four of the d quark DTQW are shown with green arrows.

A permutation matrix generates the allowed DTQW hoping of an embedded electron within the chiral condensate lattice by swapping a u quark with a d quark. The negatively charged d quark $-\frac{1}{3}$ hops in one direction, while the positively charged u quark $+\frac{2}{3}$ hops in the opposite direction. These hops directions determine the embedded electron's helicity, with the larger positive-charge quark hopping antiparallel to the electron's charge motion in this case. The symmetry allowed quark and antiquark DTQW hoppings between Wyckoff sites may occur by tunneling and preserve the embedded electron or positron quantum invariants, such as spin and helicity.

Equation 11 shows how the permutation matrix generates the embedded type I electron quantum walk along the diagonal of the sub-unit cell cube, for instance, moving from Wyckoff site (a/2, 0, a/2) to site (0, a/2, 0) (from corner 2 to 6 in the sub-cell in Figure 1a)

$$\begin{bmatrix}\psi_{\tilde{u}}\\ \psi_{u}\\ \psi_{\tilde{d}}\\ \psi_{d}\\ \psi_{\tilde{u}}\\ \psi_{d}\\ \psi_{\tilde{d}}\\ \psi_{d}\end{bmatrix} = \begin{bmatrix}1&0&0&0&0&0&0&0\\ 0&0&0&0&0&1&0&0\\ 0&0&1&0&0&0&0&0\\ 0&0&0&1&0&0&0&0\\ 0&0&0&0&1&0&0&0\\ 0&1&0&0&0&0&0&0\\ 0&0&0&0&0&0&1&0\\ 0&0&0&0&0&0&0&1\end{bmatrix}\begin{bmatrix}\psi_{\tilde{u}}\\ \psi_{d}\\ \psi_{\tilde{d}}\\ \psi_{d}\\ \psi_{\tilde{u}}\\ \psi_{u}\\ \psi_{\tilde{d}}\\ \psi_{d}\end{bmatrix} \quad \text{Eq. 11.}$$

The quark DTQW permutations may continue across adjacent unit cells within the Pmmm space group chiral condensate lattice, creating an embedded electron confinement cloud through the quantum walk. The quark DTQW permutations are assumed to occur extremely rapidly at Dirac's Zitterbewegung frequency [28]; consequently, the physical embedded electron is never bare [11] and forms an electron confinement cloud through the underlying quark and antiquark DTQW within the chiral condensate lattice. Furthermore, the embedded electron unit cell shown in Figure 3 may be deformed due to the additional electron charge, and its symmetry may differ from that of the vacuum unit cell shown in Figure 2a, which characterizes flat 'empty space'.

Figure 4 illustrates the embedded electron type II cell, which is generated by substituting a $\tilde{d}$ antiquark by a $\tilde{u}$ antiquark at Wyckoff site (0, 0, a/2) corner 7 of the chiral condensate unit sub-cell depicted in Figure 1a. The embedded electron type II cell carries a charge of -1, localized on the cube's left edge (Figure 1a). The permutation matrix swaps the $\tilde{u}$ antiquark at Wyckoff site (0, 0, a/2) with the $\tilde{d}$ antiquark at Wyckoff site (a/2, a/2, 0). As the negatively $-\frac{2}{3}$ charged $\tilde{u}$ antiquark hops from

 doi:10.20944/preprints202604.0893.v1

site (0, 0, a/2) to site (a/2, a/2, 0). The positively + $\frac{1}{3}$ charged $\tilde{d}$ antiquark hops from site (a/2, a/2, 0) to site (0, 0, a/2), their combined motion generates the second electron helicity. Here, in this case the negative charge direction aligns with the electron charge movement.

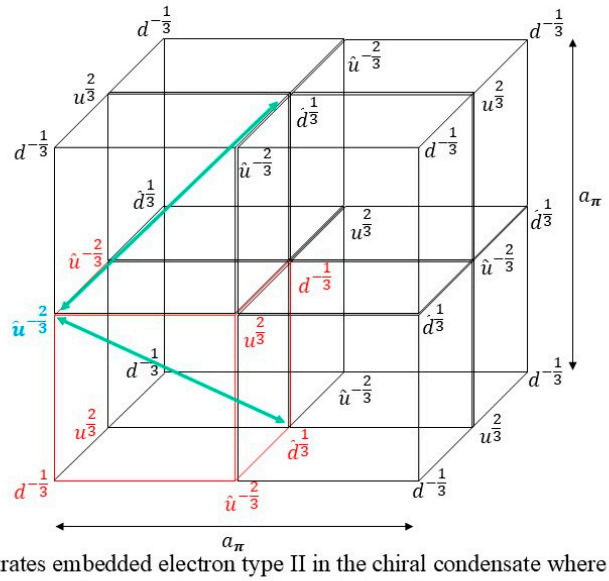

Figure 4 illustrates embedded electron type II in the chiral condensate where two possible permutations out of four possible of the $\hat{u}$ quark DTQW are shown with green arrows.

Equation 12 generates the embedded electron type II quantum walk by permutation of antiquarks along the cube's diagonal, from Wyckoff site (0, 0, a/2) to Wyckoff site (a/2, a/2, 0). Figure 4 shows two possible directions for the quantum walker, indicated by green arrows. The Pmmm space group symmetry DTQW allows four quantum paths within the chiral condensate lattice in which the embedded electron's spin and helicity are preserved. Note that for the embedded electron type II DTQW, the symmetry allowed permutations involve $\tilde{u}$ and $\tilde{d}$ antiquarks, while for the embedded electron type I, the symmetry allowed DTQW permutations involve u and d quarks.

$$\begin{bmatrix} \psi_{\tilde{u}} \\ \psi_{u} \\ \psi_{\tilde{d}} \\ \psi_{d} \\ \psi_{\tilde{u}} \\ \psi_{u} \\ \psi_{\tilde{u}} \\ \psi_{d} \end{bmatrix} = \begin{bmatrix} 1 & 0 & 0 & 0 & 0 & 0 & 0 & 0 \\ 0 & 1 & 0 & 0 & 0 & 0 & 0 & 0 \\ 0 & 0 & 0 & 0 & 0 & 0 & 1 & 0 \\ 0 & 0 & 0 & 1 & 0 & 0 & 0 & 0 \\ 0 & 0 & 0 & 0 & 1 & 0 & 0 & 0 \\ 0 & 0 & 0 & 0 & 0 & 1 & 0 & 0 \\ 0 & 0 & 1 & 0 & 0 & 0 & 0 & 0 \\ 0 & 0 & 0 & 0 & 0 & 0 & 0 & 1 \end{bmatrix} \begin{bmatrix} \psi_{\tilde{u}} \\ \psi_{u} \\ \psi_{\tilde{u}} \\ \psi_{d} \\ \psi_{\tilde{u}} \\ \psi_{u} \\ \psi_{\tilde{d}} \\ \psi_{d} \end{bmatrix} \quad \text{Eq. 12}$$

Figure 5 presents the initial configuration of the embedded positron type I unit-cell structure. This configuration is achieved by substituting a d quark at Wyckoff site (a/2, a/2, a/2) position 8 in Figure 1a, located at the center of the Pmmm unit cell, with a u quark. Four green arrows indicate allowed hopping directions for the DTQW performed by the u quark walker among the 8 symmetry allowed hops in the Pmmm lattice.

Preprints.org (www.preprints.org) | NOT PEER-REVIEWED | Posted: 14 April 2026 doi:10.20944/preprints202604.0893.v1

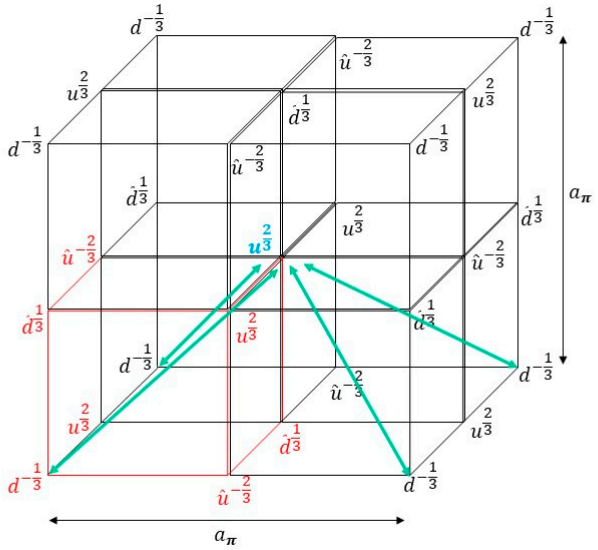

Figure 5 illustrates embedded positron type I in the chiral condensate where four possible permutations of the u quark DTQW are shown with green arrows.

Equation 13 generates the embedded positron type I permutations along the diagonal of the cube, traveling from the Pmmm Wyckoff cell center (a/2, a/2, a/2) to Wyckoff site (0, 0, 0), corner 4 within the sub-unit cell shown in Figure 1a.

$$\begin{bmatrix} \psi_{\tilde{u}} \\ \psi_{u} \\ \psi_{\tilde{d}} \\ \psi_{u} \\ \psi_{\tilde{u}} \\ \psi_{u} \\ \psi_{\tilde{d}} \\ \psi_{d} \end{bmatrix} = \begin{bmatrix} 1 & 0 & 0 & 0 & 0 & 0 & 0 & 0 \\ 0 & 1 & 0 & 0 & 0 & 0 & 0 & 0 \\ 0 & 0 & 1 & 0 & 0 & 0 & 0 & 0 \\ 0 & 0 & 0 & 0 & 0 & 0 & 0 & 1 \\ 0 & 0 & 0 & 0 & 1 & 0 & 0 & 0 \\ 0 & 0 & 0 & 0 & 0 & 1 & 0 & 0 \\ 0 & 0 & 0 & 0 & 0 & 0 & 1 & 0 \\ 0 & 0 & 0 & 1 & 0 & 0 & 0 & 0 \end{bmatrix} \begin{bmatrix} \psi_{\tilde{u}} \\ \psi_{u} \\ \psi_{\tilde{d}} \\ \psi_{d} \\ \psi_{\tilde{u}} \\ \psi_{u} \\ \psi_{\tilde{d}} \\ \psi_{u} \end{bmatrix} \quad \text{Eq. 13}$$

Figure 6 presents the embedded positron type II cell configuration, formed by substituting a $\tilde{u}$ antiquark with a $\tilde{d}$ antiquark at Wyckoff site (a/2, 0, 0), corner 5 within the sub-unit cell shown in Figure 1a. Two green arrows indicate two among the eight-symmetry allowed DTQW directions for the $\tilde{d}$ antiquark walker.

Preprints.org (www.preprints.org) | NOT PEER-REVIEWED | Posted: 14 April 2026 doi:10.20944/preprints202604.0893.v1

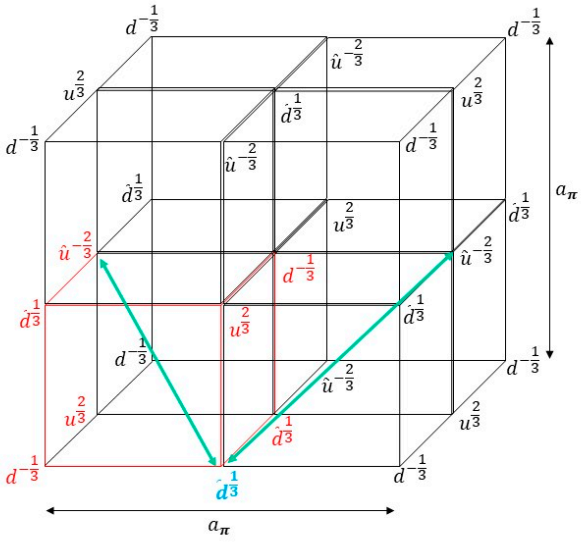

Figure 6 illustrates embedded positron type II in the chiral condensate where two possible permutations out of four of the $\hat{d}$ quark DTQW are shown with green arrows.

Equation 14 generates the embedded positron type II antiquark permutations along the cube diagonal from Wyckoff site (0, a/2, a/2), corner 1, to Wyckoff site (a/2, 0, 0) corner 5 of the sub-unit cell in Figure 1a.

$$\begin{bmatrix} \psi_{\tilde{d}} \\ \psi_u \\ \psi_{\tilde{d}} \\ \psi_d \\ \psi_{\tilde{u}} \\ \psi_u \\ \psi_{\tilde{d}} \\ \psi_d \end{bmatrix} = \begin{bmatrix} 0 & 0 & 0 & 0 & 1 & 0 & 0 & 0 \\ 0 & 1 & 0 & 0 & 0 & 0 & 0 & 0 \\ 0 & 0 & 1 & 0 & 0 & 0 & 0 & 0 \\ 0 & 0 & 0 & 1 & 0 & 0 & 0 & 0 \\ 1 & 0 & 0 & 0 & 0 & 0 & 0 & 0 \\ 0 & 1 & 0 & 0 & 0 & 1 & 0 & 0 \\ 0 & 0 & 0 & 0 & 0 & 0 & 1 & 0 \\ 0 & 0 & 0 & 1 & 0 & 0 & 0 & 1 \end{bmatrix} \begin{bmatrix} \psi_{\tilde{u}} \\ \psi_u \\ \psi_{\tilde{d}} \\ \psi_d \\ \psi_{\tilde{d}} \\ \psi_u \\ \psi_{\tilde{d}} \\ \psi_d \end{bmatrix} \quad \text{Eq. 14}$$

The examples above show how the electron spin and helicity preserved states are defined by the structure and dynamics of the Pmmm space group chiral condensate lattice. The electron spin is determined by the quantum walker quark or antiquark type (matter or antimatter), while helicity depends on whether the bigger quark charge moves parallel or antiparallel to the embedded electron's or positron's charge motion.

6. Embedded Cooper Pair Quantum Walk in the Chiral Condensate

In the chiral condensate lattice, a Cooper pair may be formed for example by replacing a u quark at Wyckoff position (a/2, 0, a/2) 2 with a d quark and a $\tilde{d}$ antiquark with a $\tilde{u}$ antiquark at Wyckoff position (0, 0, a/2) 7 in the sub-unit cell shown in Figure 1a. The two electron charges are centered on the cubic face defined by Wyckoff sites (a/2, 0, a/2) 2, (0, 0, a/2) 7, (a/2, 0, 0) 5, and (0, 0, 0) 4, creating a rectangle composed of two d quarks and two $\tilde{u}$ antiquarks. The green arrows in Figure 7 depict the coordinated movement of the two embedded electrons resulting from simultaneous symmetry allowed hoppings of quarks with the u quark and $\tilde{d}$ antiquark respectively.

Preprints.org (www.preprints.org) | NOT PEER-REVIEWED | Posted: 14 April 2026 doi:10.20944/preprints202604.0893.v1

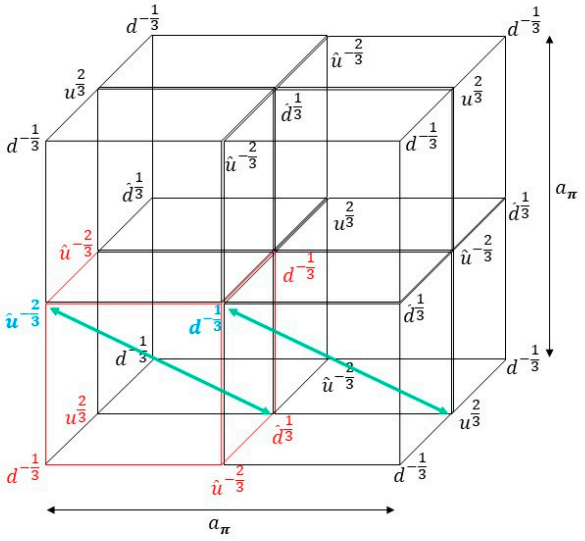

Figure 7 illustrates the motion direction of embedded Cooper pair in the chiral condensate due to d quark and $\hat{u}$ antiquark simultaneous permutations shown with green arrows .

The creation of embedded Cooper pair is described by the following matrix acting on the chiral condensate sub-unit cell depicted in Figure 1a. Specifically, at Wyckoff site (a/2, 0, a/2) a u quark is replaced by a d quark, while at Wyckoff site (0, 0, a/2), a $\tilde{d}$ antiquark is replaced by a $\tilde{u}$ antiquark.

$$\psi_{Cooper\ pair} = \begin{bmatrix} \psi_{\tilde{u}} \\ \psi_d \\ \psi_{\tilde{d}} \\ \psi_d \\ \psi_{\tilde{u}} \\ \psi_u \\ \psi_{\tilde{u}} \\ \psi_d \end{bmatrix} = \begin{bmatrix} 1 & 0 & 0 & 0 & 0 & 0 & 0 & 0 \\ 0 & 0 & 0 & 1 & 0 & 0 & 0 & 0 \\ 0 & 0 & 1 & 0 & 0 & 0 & 0 & 0 \\ 0 & 0 & 0 & 1 & 0 & 0 & 0 & 0 \\ 0 & 0 & 0 & 0 & 1 & 0 & 0 & 0 \\ 0 & 0 & 0 & 0 & 0 & 1 & 0 & 0 \\ 0 & 0 & 0 & 0 & 1 & 0 & 0 & 0 \\ 0 & 0 & 0 & 0 & 0 & 0 & 0 & 1 \end{bmatrix} \begin{bmatrix} \psi_{\tilde{u}} \\ \psi_u \\ \psi_{\tilde{d}} \\ \psi_d \\ \psi_{\tilde{u}} \\ \psi_u \\ \psi_{\tilde{d}} \\ \psi_d \end{bmatrix} \quad \text{Eq. 15}$$

The Bardeen-Cooper-Schrieffer (BCS) theory [32] explains the isotope effect in superconductors by suggesting that the coupling potential between Cooper pairs depends on lattice ion mass. In the present framework, an alternative interpretation emerges: the density and structure of the chiral condensate may depend on ion mass, whereby heavier isotopes increase the density of the chiral condensate lattice, reduce the size of the unit cells, effectively shorten Cooper pair distances, and hence strengthen their interaction.

Superconductors are used to accurately monitor variations in Earth's gravitational field resulting from the Moon's movement and Earth's orbital motion around the Sun [33,34]. Analogous to the isotope effect in superconductors, a quantum gravity theory might explain these periodic gravitational variations through periodic changes in chiral condensate density induced by the motion of the Moon and Earth. This hypothesis suggests that such density variations mediate the transmission of long-range gravitational forces, with chiral condensate density decreasing with distance from massive bodies, similar to how atmospheric density decreases with altitude above Earth's surface [31].

Preprints.org (www.preprints.org) | NOT PEER-REVIEWED | Posted: 14 April 2026 doi:10.20944/preprints202604.0893.v1

7. Embedded Electron-Positron Creation and Annihilation

Embedded electron-positron pairs may be generated within the chiral condensate by permuting for example a u quark at Wycoff position (a/2, 0, a/2) with a d quark at Wyckoff position (0, 0, 0) in the sub-unit cell depicted in Figure 1a shown in Figure 8.

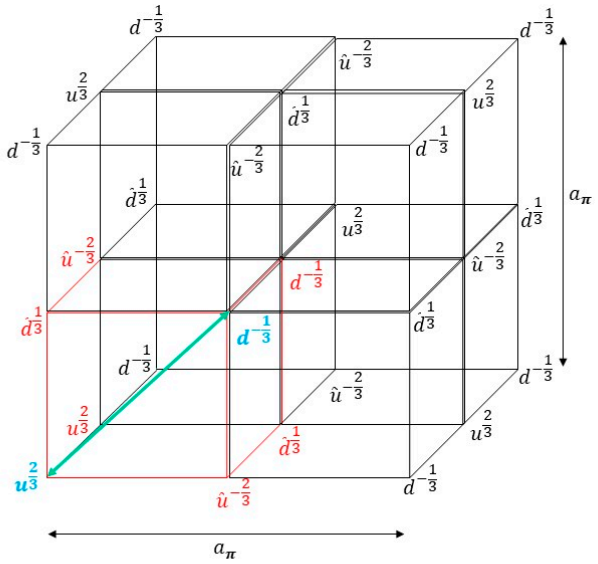

Figure 8 illustrates embedded electron-positron pair in the chiral condensate.

This permutation requires surmounting a potential barrier of 1.022 MeV, equal to twice the rest mass energy of electron. Next, the d quark in Wyckoff position (a/2, 0, a/2) can further permute with a u quark from adjacent lattice cell and similarly the u quark in Wyckoff position (0, 0, 0) can permute with a d quark from another lattice cell separating the electron and positron charges. The symmetry allowed permutations converts the neighboring unit cells into an embedded electron cell of type I (see Figure 3) and an embedded positron cell (see Figure 5). The overall result is the creation and spatial separation of an electron-positron pair within the chiral condensate lattice. Alternatively, applying the same permutation matrix a second time results in the annihilation of the electron-positron pair. The creation and annihilation processes of electron-positron pairs in the chiral condensate lattice sub-unit cell are described by Equations 16 and 17.

$$\psi_{electron-pisitron\ pair} = \begin{bmatrix} \psi_{\tilde{u}} \\ \psi_d \\ \psi_{\tilde{d}} \\ \psi_u \\ \psi_{\tilde{u}} \\ \psi_u \\ \psi_{\tilde{d}} \\ \psi_d \end{bmatrix} = \begin{bmatrix} 1 & 0 & 0 & 0 & 0 & 0 & 0 & 0 \\ 0 & 0 & 0 & 1 & 0 & 0 & 0 & 0 \\ 0 & 0 & 1 & 0 & 0 & 0 & 0 & 0 \\ 0 & 1 & 0 & 0 & 0 & 0 & 0 & 0 \\ 0 & 0 & 0 & 0 & 1 & 0 & 0 & 0 \\ 0 & 0 & 0 & 0 & 0 & 1 & 0 & 0 \\ 0 & 0 & 0 & 0 & 0 & 0 & 1 & 0 \\ 0 & 0 & 0 & 0 & 0 & 0 & 0 & 1 \end{bmatrix} \begin{bmatrix} \psi_{\tilde{u}} \\ \psi_u \\ \psi_{\tilde{d}} \\ \psi_d \\ \psi_{\tilde{u}} \\ \psi_u \\ \psi_{\tilde{d}} \\ \psi_d \end{bmatrix} \quad \text{Eq. 16}$$

$$\psi_{Pionic\ fabric} = \begin{bmatrix} \psi_{\tilde{u}} \\ \psi_u \\ \psi_{\tilde{d}} \\ \psi_d \\ \psi_{\tilde{u}} \\ \psi_u \\ \psi_{\tilde{d}} \\ \psi_d \end{bmatrix} = \begin{bmatrix} 1 & 0 & 0 & 0 & 0 & 0 & 0 & 0 \\ 0 & 0 & 0 & 1 & 0 & 0 & 0 & 0 \\ 0 & 0 & 1 & 0 & 0 & 0 & 0 & 0 \\ 0 & 1 & 0 & 0 & 0 & 0 & 0 & 0 \\ 0 & 0 & 0 & 0 & 1 & 0 & 0 & 0 \\ 0 & 0 & 0 & 0 & 0 & 1 & 0 & 0 \\ 0 & 0 & 0 & 0 & 0 & 0 & 1 & 0 \\ 0 & 0 & 0 & 0 & 0 & 0 & 0 & 1 \end{bmatrix} \begin{bmatrix} \psi_{\tilde{u}} \\ \psi_d \\ \psi_{\tilde{d}} \\ \psi_d \\ \psi_{\tilde{u}} \\ \psi_u \\ \psi_{\tilde{d}} \\ \psi_d \end{bmatrix} \quad \text{Eq. 17}$$

 doi:10.20944/preprints202604.0893.v1

The annihilation of an embedded electron-positron pair within the chiral condensate can be described also by Equation 18, in which electron and positron tetraquarks yield two neutral pion tetraquarks.

$$\tilde{u}d\tilde{d}d + u\tilde{d}\tilde{u}u \rightarrow \tilde{u}du\tilde{d} + \tilde{d}d\tilde{u}u \; Eq.(18)$$

In Equation 18, both the number and types of quarks are preserved, these reactions within the chiral condensate do not involve the creation or annihilation of quarks. It is assumed that quark-antiquark pairs are generated only in the black hole ergosphere as a result of the black hole laser effect [21,23].

8. Pmmm Ionic Lattice Analog of the Chiral Condensate Lattice

The $N_a^{+1}C_l^{-1}M_g^{+2}S^{-2}$ ionic lattice unit cell depicted in Figure 9 exhibits the same Pmmm space group structure and symmetry as the proposed chiral condensate unit cell shown in Figure 2a.

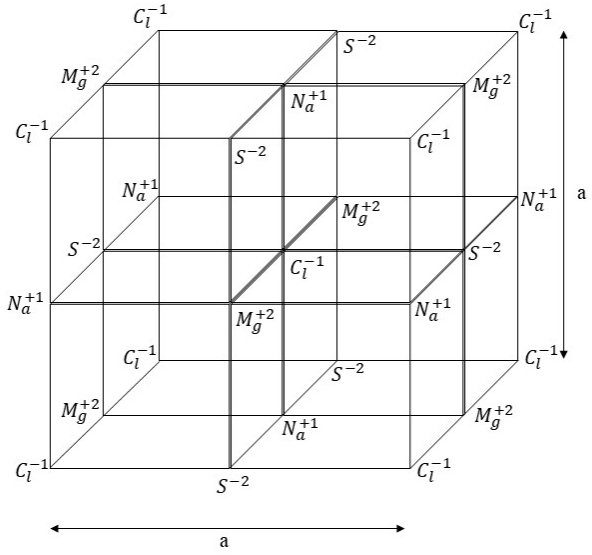

Figure 9 illustrates $N_a^{+1}C_l^{-1}M_g^{+2}S^{-2}$ ion lattice unit-cell structure analog to the chiral condensate unit-cell.

The ionic lattice of Figure 9 is not electrostatically favorable and two distinct ionic crystal phases, $N_a^{+1}C_l^{-1}$ and $M_g^{+2}S^{-2}$ are found in nature. However, in the proposed Pmmm chiral condensate unit cell, quarks and antiquarks interact through QCD strong forces. The chiral condensate melting temperature is estimated to be about Tc ≈ 155 MeV (~1.8 × 10^{12} degrees Kelvin), higher than the temperature in the core of the Sun, comparable to the temperature at the core of a supernova explosion, and exceeded only by the temperatures reached in heavy-ion collisions and at the Big Bang. The proposed Pmmm chiral condensate is probably the strongest structure that exists in nature, with a melting temperature exceeding that of stellar cores, and at the same time it is compressible and responsive, embedding composite fermions that propagate through the chiral condensate lattice by tunneling and permutations between Wyckoff sites.

9. Discrete Time Quantum Walk (DTQW) Simulations

The one-dimensional DTQW simulation results presented below demonstrate how quantum walk dynamics depends on quantum coins. Application of a Hadamard coin produces asymmetric drift of the initial Gaussian wave packet toward the left, as shown in Figure 10.

Preprints.org (www.preprints.org) | NOT PEER-REVIEWED | Posted: 14 April 2026 doi:10.20944/preprints202604.0893.v1

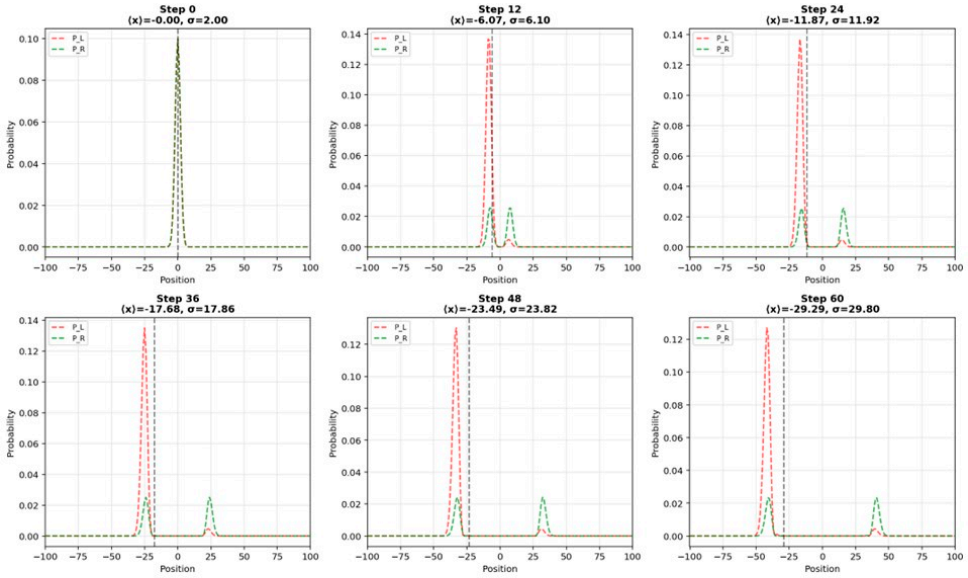

Figure 10 illustrates the one-dimensional DTQW with a Hadamard quantum coin.

Application of a symmetric coin (Eq. 19) yields symmetric DTQW evolution[13] of the two wave packet components, as shown in Figure 11.

$$C_{symmetric} = \begin{bmatrix} 1 & i \\ i & 1 \end{bmatrix} \text{ Eq. (19)}$$

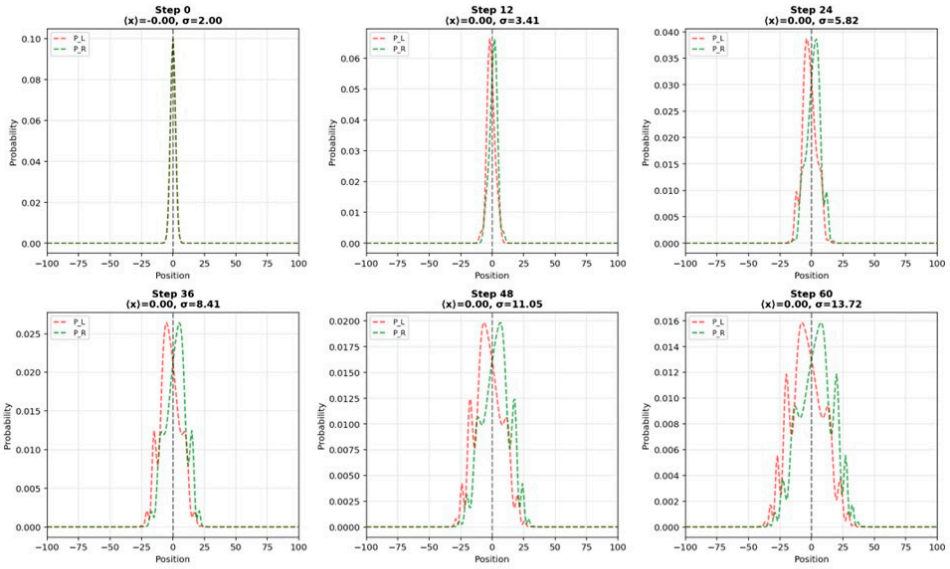

Figure 11 illustrates the one-dimensional DTQW with a Symmetric quantum coin.

A non-Hermitian coin[38] (Eq. 20) produces strongly asymmetric evolution, with markedly different dynamics for the left and right wave packet components as shown in Figure 12.

$$C_{Non-Herimtian} = \begin{bmatrix} 1 & i \\ 0 & 1 \end{bmatrix} \text{ Eq. (20)}$$

 doi:10.20944/preprints202604.0893.v1

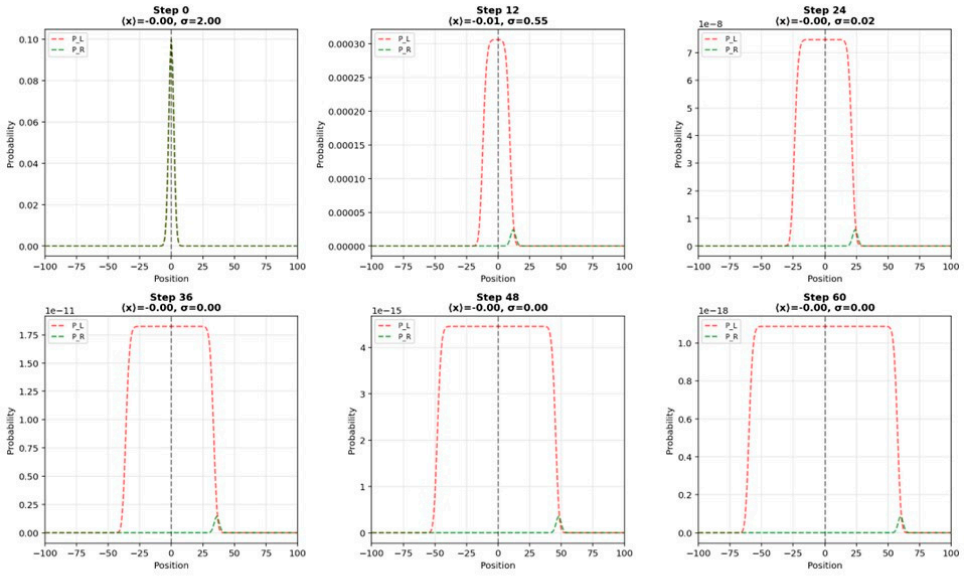

Figure 12 illustrates the one-dimensional DTQW with a non-Hermitian quantum coin.

The left wave packet component (orange color) remains centered and broadens with time, as shown with 60 time steps. The right component (green color) has significantly smaller amplitude but exhibits coherent evolution with preserved amplitude and width shown in Figure 13.

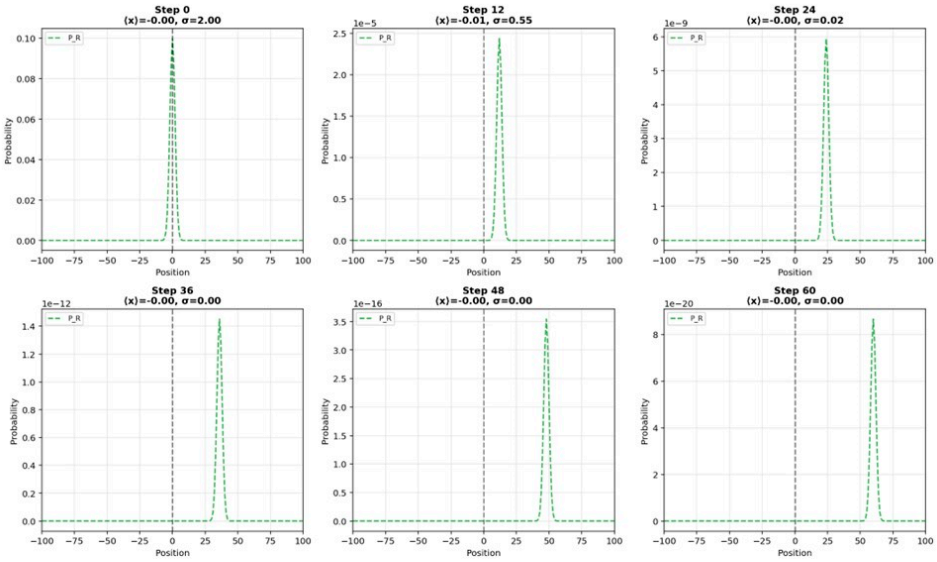

Figure 13 illustrates the right component in one-dimensional DTQW with the non-Hermitian quantum coin.

Swapping the off-diagonal quantum coin terms (Eq. 21) transfers the coherent behavior to the left wave packet component as shown in Figure 14.

$$C_{Non-Hermitian} = \begin{bmatrix} 1 & 0 \\ i & 1 \end{bmatrix} \text{Eq. (21)}$$

Preprints.org (www.preprints.org) | NOT PEER-REVIEWED | Posted: 14 April 2026 doi:10.20944/preprints202604.0893.v1

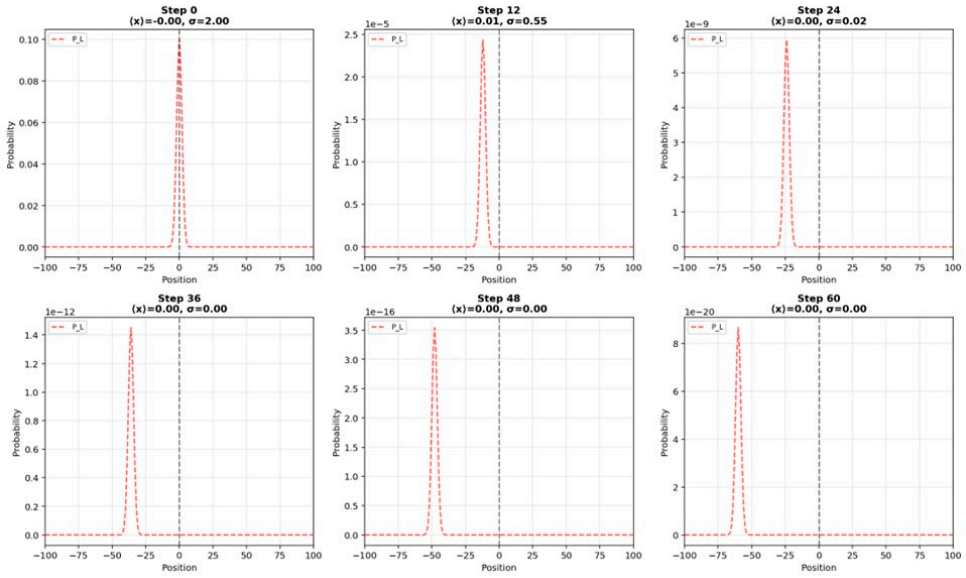

Figure 14 illustrates the left component in one-dimensional DTQW with interchanging the non-Hermitian quantum coin off-diagonal terms.

The embedded electron dynamics in the proposed Pmmm chiral condensate lattice is studied numerically using a three-dimensional discrete-time quantum walk (DTQW) simulation. The embedded electron is created by replacing a u quark at Wyckoff position u_1 = (a/2, 0, a/2) in unit cell R = 0 with a d quark as illustrated in Figure 3 above. The embedded electron then performs a DTQW by exchanging positions with neighbouring u quarks through the symmetric allowed Pmmm $d \leftrightarrow u$ hoppings. These hopping exchange reactions are two-particle events in which the substituted d quark tunnels to the u quark position in an adjacent cell while the u quark simultaneously returns to the d quark position, transferring the electron charge −1 from one cell to the next in the chiral condensate lattice.

The quantum walk state is defined as $\Psi(\mathrm{x}, \mathrm{y}, \mathrm{z}, \mathrm{direction}, \mathrm{flavour})$ with shape (N, N, N, 6, 2), where the position index (x,y,z) labels the unit cell in the N^3 supercell, the direction index runs over the six nearest-neighbour $d \leftrightarrow u$ exchange paths of the Pmmm lattice, and the flavour index distinguishes whether the substituted d quark currently occupies a u-type Wyckoff site (flavour 0, cell charge = −1) or a d-type site (flavour 1, transient). The six exchange directions are the four B-path vectors (±1, 0, ±1) in the xz face-diagonal direction, which generate the structure factor $B(k) = 4t_{du} \cos(k_x a/2) \cos(k_z a/2)$, and the two C-path vectors (0, ±1, 0) in the y direction, which generate $C(k) = t_{du} \cos(k_y a/2)$ the nearest-neighbour displacement vectors derived in the Appendix from the Pmmm space group Wyckoff geometry, and together they produce the structure factors of the quark sector Hamiltonian $\boldsymbol{H_q}(\vec{k})$ of Eq. (6a).

At each time step the quantum walk proceeds in two stages. First, the quantum coin, a 6×6 unitary matrix extended from the 4×4 quark sector Hamiltonian $\boldsymbol{H_q}(\vec{k})$ evaluated at the initial wave packet momentum k_0, mixes the amplitudes across all six direction states at every lattice site simultaneously. The quantum coin is constructed as $e^{-i\boldsymbol{H_q}(\vec{k})dt}$ where dt is the dimensionless time step, so that the B and C structure factors control the mixing strength in the xz and y directions respectively. Second, the shift operator moves each directional component to its Pmmm-constrained target cell and flips the flavour label, implementing the $d \leftrightarrow u$ exchange reactions. The shift is the permutation of the state space, preserving the norm $\|\psi\|^2 = 1$ exactly at every step and guaranteeing charge conservation.

 doi:10.20944/preprints202604.0893.v1

The initial state is a Gaussian wave packet $\Psi(r) = e^{-\frac{r^2}{2\sigma_0{}^2}} e^{-i\mathrm{k}_0 r}$ with initial width σ_0 and momentum k_0, loaded into the flavour-0 (electron) states with amplitudes weighted by the B and C structure factors of $\boldsymbol{H_q}(\overrightarrow{\mathrm{k}_0})$ to encode the initial momentum into the quantum coin degree of freedom. A Lorentz-like lattice contraction $a_x(k_x) = a_0 \sqrt{1 - \beta_x{}^2}$ is applied in the direction of the wave packet motion, so that the unit cell contracts along k_0 in analogy with special relativistic length contraction. The cell contraction reduces the structure factor argument $k_x a_x/2$, increasing $\cos(k_x a_x/2)$ toward unity and thereby strengthening the hopping coupling in the direction of motion, which enhances the directional coherence of the quantum walk.

Figure 15 compares the time evolution of the wave packet width, σ(t), against the free-space Schrödinger prediction $\sigma_{free}(t) = \sigma_0 \sqrt{1 + (\frac{t}{\tau})^2}$ derived by Darwin in 1927 for a free electron wave packet [10]. The quantum walk dynamics in the chiral condensate lattice exhibit three distinct phases. In Phase I (early steps) the wave packet spreads faster than the free-space prediction because all six hop directions simultaneously scatter amplitude away from the origin before the long-range interference pattern has been established. In Phase II the quantum interference structure imposed by the Pmmm coin, specifically the asymmetry between the four B-paths and the two C-paths, and the crossed d(1a)↔u_1 and d(1b)↔u_2 coupling pattern of $\boldsymbol{H_q}(\overrightarrow{\mathrm{k}_0})$ causes destructive interference far from the wave packet center and constructive interference near it, pulling probability back toward the origin and reducing $\sigma(t)$ below the free-space curve. In Phase III the wave packet enters a quasi-stationary coherent oscillation with a long-time average width significantly smaller than the free-space prediction. With optimized parameters, coin time step dt = 0.05, initial crystal momentum $|k_0| = 0.49\pi$ along the [1,0,0] direction, and Lorentz contraction, the DTQW simulation yields $\sigma_{final}(t) = 5.37$ at t = 80 steps compared to $\sigma_{free}(t) = 10.82$. The wave packet of the embedded electron in the Pmmm chiral condensate lattice is 50.4% more confined than a free electron wave packet over the same time interval. This confinement of the embedded electron wave packet, in contrast to the monotonic dispersal predicted by the free-space Schrödinger equation, is proposed as a direct consequence of the geometric structure of the Pmmm chiral condensate lattice: the Pmmm symmetry-constrained hopping coin $\boldsymbol{H_q}(\overrightarrow{\mathrm{k}_0})$, derived from the tight-binding Hamiltonian that produces the Pionic band structure, acts as an effective confining potential that repeatedly refocuses the electron charge distribution, providing indirect numerical evidence for the proposed role of the QCD chiral condensate lattice as the structural origin of electron confinement and coherence in the QCD vacuum.

 doi:10.20944/preprints202604.0893.v1

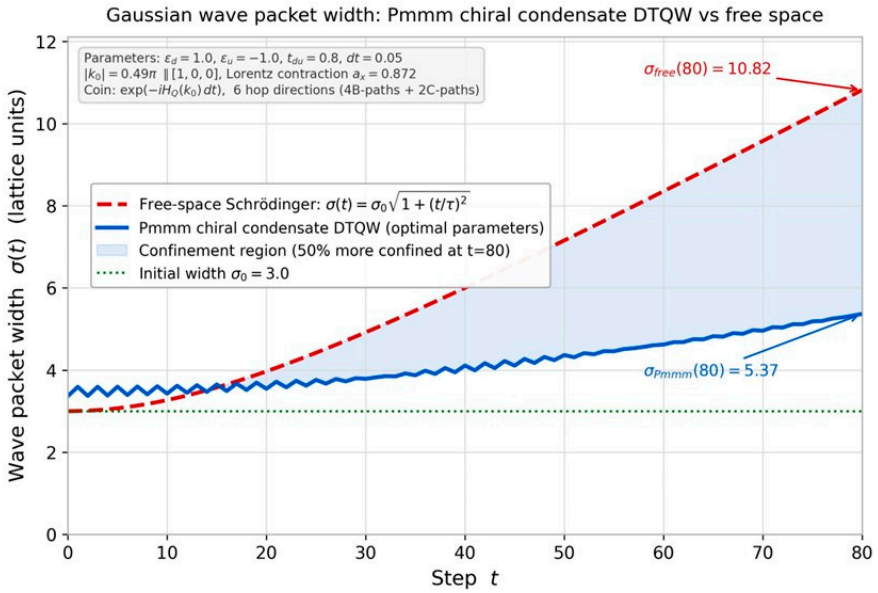

Figure 15 illustrates the improved wave-packet width with three-dimensional DTQW in the Pmmm lattice compared to free space wave-packet width dispersion

10. Discussion

The proposed Pmmm space group chiral condensate unit cell provides a concrete geometric realization of the QCD chiral condensate that complements the instanton liquid picture, proposing that quarks and antiquarks condense into an ordered Pmmm lattice with the four light quarks and antiquarks u, d, ū, $\bar{d}$ occupying the four highest-symmetry Wyckoff positions. The spontaneous reduction from the parent $Pm\bar{3}m$ cubic symmetry (No. 221, Oh, order 48) to the Pmmm subgroup (No. 47, D2h, order 8) mirrors the chiral symmetry breaking SU(2)L × SU(2)R → SU(2)V of the QCD vacuum, with the 40 broken symmetry operations generating the three pions π^+, π^-, π^0 as Goldstone bosons. In the proposed Pmmm chiral condensate lattice, the non-zero Pionic condensate VEV emerges from the geometric asymmetry of the Pmmm unit cell and is proportional to the quark hopping amplitude t_{du}. The tight-binding hopping Hamiltonian energy bands exhibit a gap at the Γ point that closes in the chiral limit, and complete band decoupling at the R point consistent with asymptotic freedom, providing quantitative support for the proposed Pmmm chiral condensate lattice.

A three-dimensional discrete-time quantum walk simulation of the embedded electron, using the quark sector Hamiltonian $\boldsymbol{H_q}(\overrightarrow{k_0})$ as the quantum coin, demonstrates that the Gaussian wave packet of the embedded electron remains 50% more confined than the free-space Schrödinger equation prediction, providing numerical evidence that the geometric structure of the Pmmm chiral condensate lattice suppresses wave packet dispersal and supports the proposed confinement of the embedded electron within the QCD chiral condensate lattice.

We propose an alternative model that could create the matter-antimatter asymmetry through spatial separation based on balanced quark reaction equations involving pion tetraquarks near black hole event horizons that preserve both the number and flavor of quarks and antiquarks (Eqs. 1-4). While anti-neutrons remain trapped below the black hole horizon, protons and electrons escape via Hawking process [22]. We assume that the chiral condensate lattice melts in the vicinity of BH horizons enabling the reaction of pion tetraquarks that produce protons, electrons and anti-neutrons. The density of the pion tetraquarks bosons may be exponentially amplified in the black hole ergosphere through the black hole laser effect [21] that may exponentially amplify the creation of deuterons and anti-deuterons in the vicinity of the BH horizons [39].

 doi:10.20944/preprints202604.0893.v1

Drawing inspiration from Harari's hypothesis that all baryonic and leptonic particles comprise four fundamental sub-entities T , V , $\tilde{T}$, $\tilde{V}$ [25] and based on insights from β decay [31], we propose that the electron is an embedded composite structure of four quarks and antiquarks $d, \tilde{u}$, d , $\tilde{d}$ and $d, \tilde{u}$, u , $\tilde{u}$. These tetraquarks are embedded within the chiral condensate lattice characterized by a Pmmm symmetry group unit cell with equal numbers of quarks and antiquarks $u, \tilde{u}$, d , $\tilde{d}$. The Pmmm chiral condensate lattice structure facilitates quark discrete-time quantum walks (DTQW) [12–19] through quarks and quarks, and separately antiquarks and antiquarks, permutations and enables the embedding of electrons, positrons, and Cooper pairs, as well as pair creation and annihilation processes without creating or annihilating quarks. Within this framework, the embedded electron spin and helicity are interpreted structurally: spin is determined by the type of quantum walker (quark or antiquark), while helicity arises from the parallel or antiparallel orientation of the larger quark charge motion relative to the electron charge motion.

Dirac suggested in his 1956 lecture "The Electron and the Vacuum" [11] that the bare electron starting point is misleading, asserting that to understand physical electron dynamics, one must develop a quantum theory for the rapidly fluctuating vacuum in its ground state, described by a wavefunction. We propose here taking another step in Dirac's line of thought by assuming that physical electrons are composite particles embedded in the chiral condensate lattice and hence are never bare. We suggest that the embedded electrons form confined clouds within the chiral condensate lattice due to rapid underlying quark and antiquark DTQW permutations via tunneling from site to site, occurring at the Zitterbewegung frequency [28].

Melnikov and Fedichkin, in "Quantum Walks of Interacting Fermions on a Cycle Graph" [18] concluded that although general quantum walk electron dynamics in a circle are aperiodic, given sufficient time, an arbitrary precision of return to the initial state is guaranteed by the Poincaré recurrence theorem [35,36]. Returning to the proposed embedded electron DTQW in the chiral condensate lattice, we assume that the underlying quark permutations create electron confined clouds that restore the spinor wavefunction to its initial state at Poincaré recurrence times, preserving the coherence. We propose that an electron undergoing a discrete-time quantum walk (DTQW) embedded within the chiral condensate lattice produces a coherent wave packet. The confinement of electrons as opposed to the wave packet dispersion found by Schrödinger and Darwin in 1927 [9,10] may provide indirect evidence for the existence of the proposed Pmmm chiral condensate lattice structure and the embedded composite electrons.

Acknowledgments: The author would like to thank Prof. Aharon Davidson for helpful discussions.:

Abbreviations

The following abbreviations are used in this manuscript:

DTQW	Discrete Time Quantum Walk
QCD	Quantum Chromodynamics
QFT	Quantum Field Theory
SM	Standard Model

Appendix

The Chiral Condensate Lattice Tight-Binding Hopping Hamiltonian Model

The Appendix provides detailed derivation of the tight-binding symmetric analytical solvable Hamiltonian model based on the geometric structure of the proposed Pmmm chiral condensate unit cell. The derivation of Eqs. (6a-e) proceeds through the following steps:

1. Identify the eight Pmmm space group Wyckoff positions: d quark at Wyckoff 1a (0,0,0) + 1b (a/2,a/2,a/2); u quark at Wyckoff 3c representative (a/2,0,a/2) and (0,a/2,0); $\tilde{d}$ at (a/2,a/2,0) and (0,0,a/2); and $\tilde{u}$ at (a/2,0,0) and (0,a/2,a/2).

 doi:10.20944/preprints202604.0893.v1

2. Introduce the tight-binding Hamiltonian model for the chiral condensate Pmmm space group lattice.

3. Introduce the hopping selection rules ($d \leftrightarrow u$ and $\tilde{d} \leftrightarrow \tilde{u}$ only), setting all other hopping amplitudes to zero generating the symmetric analytically solvable block-diagonal Hamiltonian: $H(k) = H_q(k) \oplus H_{\tilde{q}}(k)$.

4. Calculate the structure factors with the allowed hopping selection rules with nearest-neighbor approximation: B = $4t_{du}cx\ cz$, C = $2\ t_{du}cy$, F = $4\ t_{\tilde{d}\tilde{u}}\ cx\ cy$, G = $2\ t_{\tilde{d}\tilde{u}}\ cz$.

5. Introduce the decoupled 4×4 quark block H_q and antiquark block $H_{\tilde{q}}$.

6. Calculate analytically the energy bands by diagonalization of the 4×4 block symmetric Hamiltonian using symmetric/antisymmetric basis unitary transformation.

A.1 The Pmmm space group eight high-symmetry Wyckoff positions

The complete set of lattice points for each species within the conventional unit cell (including all boundary-shared points) is identified bellow. The proposed QCD chiral condensate lattice has a cubic unit cell of side a with space group Pmmm (No. 47, point group D2h, order 8). This cell is assumed to arise by symmetry breaking from the parent cubic space group Pm3¯m (No. 221, point group Oh, order 48) upon condensation of the four light quark flavors $u, \tilde{u}, d, \tilde{d}$ into the high-symmetry Wyckoff positions.

d quark (Wyckoff 1a + 1b): (0,0,0), (a,0,0), (0, a,0), (0,0, a), (0, a, a), (a, a,0), (a,0, a), (a, a, a) and (a/2, a/2, a/2)

The Wyckoff 1a site at (0,0,0) has site symmetry Oh (the full octahedral group, order 48), the highest possible site symmetry in Pm3¯m. The Wyckoff 1b site at (a/2, a/2, a/2) has the same site symmetry Oh. Both are invariant under all 48 symmetry operations of the parent cubic group, making the d quark a scalar singlet under the cubic point group.

$\tilde{d}$ antiquark (Wyckoff 3d, z-direction): (0, 0, a/2), (a, 0, a/2), (0, a, a/2), (a, a, a/2), (a/2 ,a/2, 0), (a/2, a/2, a)

The representative internal position is (a/2, a/2, 0) in fractional coordinates (½, ½, 0). The site symmetry of the 3d position in Pm3¯m is D4h (order 16). The three members of positions (0, ½, ½), (½, 0, ½), (½, ½, 0) in fractional coordinates, transform as the T1u polar vector representation of Oh. The $\tilde{d}$ antiquark is associated with the z-component of this triplet.

u quark (Wyckoff 3c, xz-direction): (0, a/2,0), (a, a/2,0), (0, a/2, a), (a, a/2, a), (a/2 ,0, a/2), (a/2, a, a/2)

The representative internal position is (½, 0, ½) in fractional coordinates, which is the xz-face center. The u quark is associated with the xz-component of the T1u polar vector triplet.

$\tilde{u}$ antiquark (Wyckoff 3d, x-direction): (a/2,0,0), (a/2,a,0), (a/2,0,a), (a/2,a,a), (0,a/2,a/2), (a,a/2,a/2).

Wyckoff assignments for the four quark species in the Pmmm unit cell

Species	Wyckoff position	Representative position	Site symmetry	Per cell
d	1a + 1b	(0,0,0) and (a/2, a/2, a/2)	Oh (order 48)	2
$\tilde{d}$	3d (z-direction)	(a/2, a/2,0)	D4h (order 16)	2
u	3c (xz-direction)	(a/2, 0, a/2)	D4h (order 16)	2
$\tilde{u}$	3d (x-direction)	(a/2, 0, 0)	D4h (order 16)	2
Total				**8**

 doi:10.20944/preprints202604.0893.v1

The proposed unit cell contains 8 quark/antiquark positions per primitive cell: $2d$+ $2\tilde{u}$+$2u$+ $2\tilde{d}$.

A.2 The Tight-Binding Hamiltonian Model

The tight-binding Hamiltonian in second-quantized form is written as [29,40]:

$$H = H_{on-site} \oplus H_{hop} \; Eq.A1$$

The on-site part assigns an energy ε_α to each quark flavor $\alpha \in \{d, u, \tilde{d}, \tilde{u}\}$, representing the effective single-particle energy of that species at its Wyckoff position:

$$H_{on-site} = \varepsilon_d \sum C^\dagger_{d,R,i} C_{d,R,i} + \varepsilon_u \sum C^\dagger_{u,R,j} C_{u,R,j} + \varepsilon_{\tilde{d}} \sum C^\dagger_{\tilde{d},R,k} C_{\tilde{d},R,k} + \varepsilon_{\tilde{u}} \sum C^\dagger_{\tilde{u},R,l} C_{\tilde{u},R,l} \quad Eq.A2$$

where R labels the primitive cell index and i, j label the two inequivalent sites of each species within the cell. The index i = 1 refers to the Wyckoff 1a-type site (corner-derived) and i = 2 to the Wyckoff 1b-type site (body-center-derived) for the d quark; similarly j = 1 refers to the xz-face-center site and j = 2 to the y-edge-midpoint site for the u quark and similarly the k and l indexes represent the two positions of the $\tilde{d}$ and $\tilde{u}$ antiquarks.

The hopping part describes the quantum mechanical amplitude for a quark to tunnel from one Wyckoff site to a neighboring Wyckoff site:

$$H_{hop} = -\sum_{R,R'} \sum_{\alpha\beta} t_{\alpha\beta}(R - R') \, C^\dagger_{\alpha,R} C_{\beta,R'} + \text{h.c.} \; Eq.A3$$

where $t_{\alpha\beta}(R - R')$ is the hopping integral from species β at cell R′ to species α at cell R. The hopping integrals are determined by the overlap of the quark wavefunctions at the two sites, which depends on both the distance and the symmetry of the path between them.

A.3 The Hopping Selection Rules

We assume that the only symmetry allowed hoppings are: $d \leftrightarrow u$ (quark sector hopping) and $\tilde{d} \leftrightarrow \tilde{u}$ (antiquark sector hopping) where both d and u quarks and $\tilde{d}$ and $\tilde{u}$ antiquark numbers are conserved in these quark exchange reactions. As shown below, these selection rules decouple the tight-binding hoppings Hamiltonian model. Under these selection rules only two hopping amplitudes are non-zero:

t_{du}: $d \leftrightarrow u$ hopping amplitude (quark sector)

$t_{\tilde{d}\tilde{u}}$: $\tilde{d} \leftrightarrow \tilde{u}$ hopping amplitude (antiquark sector)

All other hopping amplitudes: $t_{d\tilde{u}}$, $t_{d\tilde{d}}$, $t_{u\tilde{u}}$, $t_{u\tilde{d}}$, t_{dd}, t_{uu}, $t_{\tilde{d}\tilde{d}}$, $t_{\tilde{u}\tilde{u}}$ are set to zero in the model producing a block-diagonal Hamiltonian model:

$$H = H_q \oplus H_{\tilde{q}} \; Eq.A4$$

where H_q operates in the {d,u} quark subspace and $H_{\tilde{q}}$ operate in the {$\tilde{d}$,$\tilde{u}$} antiquark subspace.

A.4 Structure Factor Calculation with Nearest-Neighbors Approximation

According to Bloch theorem [40], the eigenstates of a periodic Hamiltonian can be written as Bloch waves:

$$|k, \alpha\rangle = \frac{1}{\sqrt{N}} \sum_R e^{ik\,(R+\tau\alpha)} \, C^\dagger(\alpha_R) \, |0\rangle \; Eq.A5$$

where R is the Bravais lattice vector of primitive cell R, $\tau\alpha$ is the position of site α within the lattice cell, and N is the total number of cells. In the Bloch basis the hopping Hamiltonian matrix element between species α and β is:

$$H_{\alpha\beta} = \langle k, \alpha | H | k, \beta \rangle = \sum_{\Delta R} t_{\alpha\beta}(\Delta R) e^{ik\,(\Delta R + \tau\beta - \tau\alpha)} \quad Eq.A6$$

 doi:10.20944/preprints202604.0893.v1

where ΔR = R′ − R is the lattice vector difference. In the nearest-neighbor approximation, only the shortest displacement vectors $\delta = \Delta R + \tau\beta - \tau\alpha$ contribute, and the hopping amplitude $t_{\alpha\beta}$ is assumed equal for equivalent neighbors. The Hamiltonian matrix element then simplifies to the structure factor:

$$H_{\alpha\beta}(k) = f_{\alpha\beta}(k) = t_{\alpha\beta} \sum_{\delta} e^{ik\delta} \quad Eq.A7$$

where the sum runs over all nearest-neighbor displacement vectors δ connecting a Wyckoff site β to Wyckoff site α. For centrosymmetric lattices such as Pmmm, the structure factors are real, because every hop vector δ is accompanied by its inversion-related symmetric partner $-\delta$, and $e^{ik\delta}$ + $e^{-ik\delta}$= $2\cos(k\delta)$ is real. For the Pmmm chiral condensate lattice the cosine factors appear with arguments $\frac{ka}{2}$ because the nearest-neighbor vectors between Wyckoff sites are of magnitude $\frac{a}{2}$, half the lattice constant. cx, cy and cz are defined as:

$$\text{cx} = \cos(k_x a/2),\ \text{cy} = \cos(k_y a/2) \text{ and } \text{cz} = \cos(k_z a/2) \quad Eq.A8$$

Structure Factor B(k): d ↔ u Hopping via the xz Face-Diagonal

Site d_{1a} at Wyckoff 1a: $\tau_{d_{1a}} = (0,0,0)$

Site u_1 at Wyckoff 3c: $\tau_{u_1} = (\frac{a}{2}, 0, \frac{a}{2})$ [xz face-center representative]

Both sites belong to the same primitive cell R = 0. The intra-cell displacement vector from $d_{1a}$to u_1 is:

$$\tau_{u_1} - \tau_{d_{1a}} = \left(\frac{a}{2}, 0, \frac{a}{2}\right) - (0,0,0) = \left(\frac{a}{2}, 0, \frac{a}{2}\right)$$

There are four equivalent displacement vectors:

$$n_1 = 0,\ n_3 = 0:\ \delta = \left(+\frac{a}{2}, 0, +\frac{a}{2}\right),\ |\delta| = a/\sqrt{2}$$

$$n_1 = -1,\ n_3 = 0:\ \delta = \left(-\frac{a}{2}, 0, +\frac{a}{2}\right),\ |\delta| = a/\sqrt{2}$$

$$n_1 = 0,\ n_3 = -1:\ \delta = \left(+\frac{a}{2}, 0, -\frac{a}{2}\right),\ |\delta| = a/\sqrt{2}$$

$$n_1 = -1,\ n_3 = -1:\ \delta = \left(-\frac{a}{2}, 0, -\frac{a}{2}\right),\ |\delta| = a/\sqrt{2}$$

The 4 displacement vectors lie in the xz plane (y = 0 component), reflecting the xz-type character of the 3c Wyckoff position occupied by u_1.

The structure factor B(k) is the sum $e^{ik\delta}$ over all 4 nearest-neighbor vectors, multiplied by the hopping amplitude t_{du}:

$$B(k) = t_{du}\left[e^{(\frac{ik_x a}{2}+\frac{ik_z a}{2})} + e^{(-\frac{ik_x a}{2}+\frac{ik_z a}{2})} + e^{(\frac{ik_x a}{2}-\frac{ik_z a}{2})} + e^{(-\frac{ik_x a}{2}-\frac{ik_z a}{2})}\right]$$

$$B(k) = t_{du}\left[e^{(\frac{ik_x a}{2})} + e^{(-\frac{ik_x a}{2})}\right]\left[e^{(\frac{ik_z a}{2})} + e^{(-\frac{ik_z a}{2})}\right]$$

$$B(\text{k}) = 4t_{du}\cos(k_x a/2)\cos(k_z a/2) = 4t_{du}\,cx\ cz \quad Eq.A9$$

Structure Factor C(k): d ↔ u Hopping via the y Direction

Site d_{1a} at Wyckoff 1a: $\tau_{d_{1a}} = (0,0,0)$

Site u_2 at Wyckoff 3c: $\tau_{u_2} = (0, \frac{a}{2}, 0)$ [y-edge midpoint representative]

 doi:10.20944/preprints202604.0893.v1

$\tau_{u_2} - \tau_{d_{1a}} = \left(0, \frac{a}{2}, 0\right) - (0,0,0) = 0, \frac{a}{2}, 0)$

There are two equivalent displacement vectors:

n_1=0, n_2=0, n_3=0: $\delta = \left(0, +\frac{a}{2}, 0\right)$, |δ| = a/2

n_1=0, n_2=−1, n_3=0: $\delta = \left(0, -\frac{a}{2}, 0\right)$, |δ| = a/2

$$C(k) = t_{du}\left[e^{\left(\frac{ik_y a}{2}\right)} + e^{\left(-\frac{ik_y a}{2}\right)}\right] = 2\, t_{du} \cos\left(k_y a/2\right) = 2\, t_{du} cy \; Eq.A10$$

Structure Factor F : $\tilde{d}_1 \leftrightarrow \tilde{u}_1$ Hopping via the xy Face-Diagonal

Site $\tilde{d}_1$ is at (a/2, a/2, 0) (xy-face center). Site $\tilde{u}_1$ is at (a/2, 0, 0) (x-edge midpoint). The nearest-neighbor displacement vectors connecting these two site types lie in the xy plane:

δ = (±a/2, ±a/2, 0) 4 xy face-diagonal vectors

There are four equivalent displacement vectors:

The Fourier sum similar to B(k) calculation above gives:

$$\mathrm{F(k)} = 4\, t_{\tilde{d}\tilde{u}}\, cx\, cy$$

Note that the structure factor F involves cx and cy the xy face-diagonal in contrast to the quark sector B factor which involves cx and cz. This xy vs xz distinction is the direct geometric consequence of the antiquark species occupying a different set of Wyckoff positions.

Structure Factor G : $\tilde{d}_1 \leftrightarrow \tilde{u}_2$ Hopping via the z Direction

Site $\tilde{u}_2$ is at (0, a/2, a/2) (yz-face centre). The displacement vectors from $\tilde{d}_1$ at (a/2, a/2, 0) to $\bar{u}_2$ involve z-direction hops:

There are tow equivalent displacement vectors:

δ = (0, 0, ±a/2) 2 z-direction vectors

$$\mathrm{G(k)} = 2\, t_{\tilde{d}\tilde{u}}\, cz \; Eq.A11$$

The antiquark G factor involves cz alone corresponding to z-direction hopping while the quark sector C factor involves cy alone. The substitution y ↔ z relative to the quark sector reflects the axis permutation in the Pmmm unit cell between the quark and antiquark Wyckoff positions.

The Inversion-Symmetry Cross-Coupling Pattern

The structure factors for $d_{1\mathrm{b}}$ are obtained by the same Fourier sum, but starting from $\tau_{d_{1b}} = (a/2, a/2, a/2)$ instead of $\tau_{d_{1a}} = (0,0,0)$. The key result derivable by an identical calculation is that the roles of B and C are crossed for $d_{1\mathrm{b}}$ compared to $d_{1\mathrm{a}}$ position:

$d_{1\mathrm{a}}$ ↔ u_1: structure factor B = $4t_{du} cx\, cz$

$d_{1\mathrm{a}}$↔ u_2: structure factor C = $2\, t_{du} cy$

$d_{1\mathrm{b}}$ ↔ u_1: structure factor C = $2\, t_{du} cy$

$d_{1\mathrm{b}}$↔ u_2: structure factor B = $4t_{du} cx\, cz$

This inversion symmetry is mandated by the Pmmm space group: the inversion operation i maps (x, y, z) → (−x, −y, −z), which maps $d_{1\mathrm{a}}$ at (0,0,0) ↔ $d_{1\mathrm{b}}$ at (a/2,a/2,a/2) [related by inversion through the sub-cell center (a/4,a/4,a/4) shown in Figure 1a] and simultaneously maps u_1 at (a/2,0,a/2) ↔ u_2 at (0,a/2,0). Inversion therefore swaps both the d-site labels and the u-site labels, crossing the coupling assignments. This crossed pattern produces the distinctive off-diagonal block structure of $\boldsymbol{H_q}(\vec{k})$ shown in Section A.4, and the inversion symmetry generates the symmetric/antisymmetric band splitting B ± C that appears in the energy bands.

A.5 The decoupled 4×4 Quark Block $\boldsymbol{H_q}$ and antiquark block $\boldsymbol{H_{\tilde{q}}}$

Assembling the structure factors into the 4×4 quark block, with basis ordering $|d_{1a}\rangle$, $|d_{1b}\rangle$, $|u_1\rangle$, $|u_2\rangle$:

 doi:10.20944/preprints202604.0893.v1

$$\boldsymbol{H_q}(\vec{k}) = \begin{vmatrix} \varepsilon_d & 0 & 4t_{du}cx\,cz & 2t_{du}\mathrm{cy} \\ 0 & \varepsilon_d & 2t_{du}\mathrm{cy} & 4t_{du}cx\,cz \\ 4t_{du}cx\,cz & 2t_{du}\mathrm{cy} & \varepsilon_u & 0 \\ 2t_{du}\mathrm{cy} & 4t_{du}cx\,cz & 0 & \varepsilon_u \end{vmatrix} \quad Eq.A12$$

The antiquark sector is derived analogously, but the geometric roles of the coordinate axes are permuted. The $\tilde{d}$ antiquark occupies the z-direction 3d position while $\tilde{u}$ occupies the x-direction 3d position. This axis permutation produces a different pair of structure factors. The structure factors with basis ordering $|\tilde{d}_1\rangle$, $|\tilde{d}_2\rangle$, $|\tilde{u}_1\rangle$, $|\tilde{u}_2\rangle$:

$$\boldsymbol{H_{\tilde{q}}}(\vec{k}) = \begin{vmatrix} \varepsilon_{\tilde{d}} & 0 & 4t_{\tilde{d}\tilde{u}}cx\,cy & 2t_{\tilde{d}\tilde{u}}\mathrm{cz} \\ 0 & \varepsilon_{\tilde{d}} & 2t_{\tilde{d}\tilde{u}}\mathrm{cz} & 4t_{\tilde{d}\tilde{u}}cx\,cy \\ 4t_{\tilde{d}\tilde{u}}cx\,cy & 2t_{\tilde{d}\tilde{u}}\mathrm{cz} & \varepsilon_{\tilde{u}} & 0 \\ 2t_{\tilde{d}\tilde{u}}\mathrm{cz} & 4t_{\tilde{d}\tilde{u}}cx\,cy & 0 & \varepsilon_{\tilde{u}} \end{vmatrix} \quad Eq.A13$$

A.6 The Energy Bands Calculation

Each 4×4 block can be diagonalized analytically by exploiting the $Z_2 \times Z_2$ symmetry of the block: both $\boldsymbol{H_q}$ and $\boldsymbol{H_{\tilde{q}}}$ are invariant under the simultaneous exchange $d_{1a} \leftrightarrow d_{1b}$ combined with $u_1 \leftrightarrow u_2$ (or $\tilde{d}_1 \leftrightarrow \tilde{d}_2$ combined with $\tilde{u}_1 \leftrightarrow \tilde{u}_2$). This symmetry is generated by the Pmmm inversion operation which maps each Wyckoff site to its inversion-related partner as seen in Figure 1a and Figure 1b.

The unitary symmetric (+) and antisymmetric (−) transformation is:

$$\begin{aligned} |d^+\rangle &= (|d_{1a}\rangle + |d_{1b}\rangle)/\sqrt{2} \\ |d^-\rangle &= (|d_{1a}\rangle - |d_{1b}\rangle)/\sqrt{2} \\ |u^+\rangle &= (|u_1\rangle + |u_2\rangle)/\sqrt{2} \\ |u^-\rangle &= (|u_1\rangle - |u_2\rangle)/\sqrt{2} \end{aligned}$$

In the symmetric and antisymmetric basis the 4×4 quark block becomes block-diagonal after the unitary transformation $\boldsymbol{H_q}' = \mathrm{U}\ \boldsymbol{H_q}\ \mathrm{U}^{\mathrm{T}}$, separating into two independent 2×2 matrices H_+ and H_-:

$$\boldsymbol{H\_q}'(\vec{k}) = \begin{vmatrix} \varepsilon_d & 0 & 4t_{du}cx\,cz + 2t_{du}\mathrm{cy} & 0 \\ 0 & \varepsilon_d & 0 & 4t_{du}cx\,cz - 2t_{du}\mathrm{cy} \\ 4t_{du}cx\,cz + 2t_{du}\mathrm{cy} & 0 & \varepsilon_u & 0 \\ 0 & 4t_{du}cx\,cz - 2t_{du}\mathrm{cy} & 0 & \varepsilon_u \end{vmatrix} \quad Eq.A14$$

Symmetric Quark Block ($|\mathbf{d}^+\rangle$, $|\mathbf{u}^+\rangle$)

$$H_+ = \begin{vmatrix} \varepsilon_d & 4t_{du}cx\,cz + 2t_{du}\mathrm{cy} \\ 4t_{du}cx\,cz + 2t_{du}\mathrm{cy} & \varepsilon_u \end{vmatrix} \quad Eq.A15$$

The off-diagonal element $B + C = 4t_{du}cx\,cz + 2t_{du}\mathrm{cy} = 2t_{du}\ (2cx\,cz + \mathrm{cy})$.

The eigenvalues of the 2×2 H_+ symmetric matrix is:

$$E_{1,2} = \frac{\varepsilon_d+\varepsilon_u}{2} \pm \sqrt{\left(\frac{\varepsilon_d-\varepsilon_u}{2}\right)^2 + (2t_{du})^2(2\,cx\,cz + cy)^2} \quad Eq.A16$$

Antisymmetric Quark Block ($|\mathbf{d}^-\rangle$, $|\mathbf{u}^-\rangle$)

$$H_- = \begin{vmatrix} \varepsilon_d & 4t_{du}cx\,cz - 2t_{du}\mathrm{c} \\ 4t_{du}cx\,cz - 2t_{du}\mathrm{c} & \varepsilon_u \end{vmatrix} \quad Eq.A17$$

The off-diagonal element is $B - C = 4t_{du}cx\,cz - 2t_{du}\mathrm{cy} = 2t_{du}\ (2cx\,cz - \mathrm{cy})$.

The eigenvalues of the 2×2 H_- anti-symmetric matrix is:

$$E_{3,4} = \frac{\varepsilon_d+\varepsilon_u}{2} \pm \sqrt{\left(\frac{\varepsilon_d-\varepsilon_u}{2}\right)^2 + (2t_{du})^2(2\,cx\,cz - cy)^2} \quad Eq.A18$$

Antiquark Bands

The same procedure applied to $\boldsymbol{H_{\tilde{q}}}$ with symmetric/antisymmetric combinations of $|\tilde{d}^+\rangle$, $|\tilde{d}^-\rangle$, $|\tilde{u}^+\rangle$ and $|\tilde{u}^-\rangle$ gives:

off-diagonal element $F + G = 4t_{\tilde{d}\tilde{u}}cx\,cy + 2t_{\tilde{d}\tilde{u}}\mathrm{cz} = 2t_{\tilde{d}\tilde{u}}(2cx\,cy + cz)$:

$$E_{5,6} = \frac{\varepsilon_{\tilde{d}}+\varepsilon_{\tilde{u}}}{2} \pm \sqrt{\left(\frac{\varepsilon_{\tilde{d}}-\varepsilon_{\tilde{u}}}{2}\right)^2 + (2t_{\tilde{d}\tilde{u}})^2(2\,cx\,cy + cz)^2} \quad Eq.A19$$

off-diagonal element $F - G = 4t_{\tilde{d}\tilde{u}}cx\,cy - 2t_{\tilde{d}\tilde{u}}\mathrm{cz} = 2t_{\tilde{d}\tilde{u}}(2cx\,cy - cz)$:

 doi:10.20944/preprints202604.0893.v1

$$E_{7,8} = \frac{\mathcal{E}_{\tilde{d}} + \mathcal{E}_{\tilde{u}}}{2} + -\sqrt{\left(\frac{\mathcal{E}_{\tilde{d}} - \mathcal{E}_{\tilde{u}}}{2}\right)^2 + (2t_{\tilde{d}\tilde{u}})^2(2\,cx\,cy - cz)^2} \quad Eq.A20$$

K-Space high-symmetry point behavior

At k-space Γ point (kx = ky = kz = 0): cx = cy = cz = 1, giving B + C = $6t_{du}$ and B − C = $2t_{du}$. The symmetric and antisymmetric bands are split by $4t_{du}$, which may represent the chiral condensate lattice mass analog of the QCD pion mass m_π.

At k-space X point (kx = π/a, ky = kz = 0): cx = 0, cy = cz = 1. Then B = 0 and C = $2t_{du}$, giving B + C = B − C = C. The symmetric and antisymmetric bands are degenerate at the X point.

At k-space R point (k = (π/a, π/a, π/a)): cx = cy = cz = 0. All structure factors vanish: B = C = F = G = 0. All eight bands collapse to the four on-site energies, complete decoupling of all sites at the Brillouin zone corner.

Adding a Lorentz contraction to the k-space Hamiltonian

Note that the structure factors $4t_{du}cx\,cz$ and $2t_{du}cy$ depend on cosines functions of the momentum in the x, y and z directions, $\mathrm{cx} = \cos(k_x a/2)$, $\mathrm{cy} = \cos(k_y a/2)$ and $\mathrm{cz} = \cos(k_z a/2)$. If we assume that the chiral condensate lattice length contracts in the direction of motion of the embedded particle with a Lorentz contraction, $a_x = a_x(k_x)$, $a_y = a_y(k_y)$, $a_z = a_z(k_z)$, the embedded electron performing a quantum walk in the Pmmm chiral condensate lattice velocity in the x direction for example will increase since the cosine term will increase reaching the limit value of 1 with higher k_x momentum. A three-dimensional DTQW simulation of the embedded electron in the proposed Pmmm QCD chiral condensate lattice will be presented in a future work.

Appendix Summary

The tight-binding hopping Hamiltonian constructed for the Pmmm unit cell, constrained by the Pmmm symmetry and the hopping selection rules ($d \leftrightarrow u$, $\tilde{d} \leftrightarrow \tilde{u}$ allowed, all other hoppings forbidden), yields an 8×8 k-space Hamiltonian that is real, symmetric, and analytically solvable, and is block-diagonal in two 4×4 sectors. Each 4×4 block further decomposes into two analytically solvable 2×2 matrices via the symmetric and antisymmetric transformation of the two equivalent sites within each sector. The resulting eight closed-form energy bands are a direct consequence of the Pmmm space group geometry and the enforced hopping selection rules.

The proposed Pmmm space group chiral lattice unit cell of Figure 2a may be the geometric framework for the QCD chiral condensate. The condensation of the four quarks $\tilde{u}\,u\,d\,\tilde{d}$ into specific high symmetry Wyckoff positions reduces the space group symmetry from Pm3¯m (No. 221, point group Oh, order 48) to Pmmm (No. 47, point group D2h, order 8). The geometric symmetry breaking of the Pm3¯m to Pmmm space group, may play the role of the spontaneous breaking of the chiral symmetry group SU(2)L × SU(2)R → SU(2)V that characterizes the QCD vacuum. According to Goldstone's theorem, each continuously broken symmetry generator produces one massless Goldstone boson. The three broken rotational directions of the cube, the three independent ways of rotating between x, y, z that are no longer symmetries in Pmmm space group, correspond to three independent broken generators, producing three Goldstone bosons. The multiplicity-3 of the Wyckoff positions 3c and 3d, which transforms as the T1u irreducible representation of Oh, a polar vector representation provides the geometric origin of the SU(2) isospin triplet structure of the pion field. The QCD pion triplet is encoded in the geometry of the Pm3¯m to Pmmm symmetry reduction at the level of the proposed lattice structure of the chiral condensate lattice of the vacuum.

The proposed Pmmm chiral condensate unit cell of Figure 2a may provide the geometric framework for the QCD chiral condensate. The condensation of the four light quarks and antiquarks $\tilde{u}\,u\,d\,\tilde{d}$ into specific high-symmetry Wyckoff positions reduces the space group symmetry from Pm3¯m (No. 221, point group Oh, order 48) to Pmmm (No. 47, point group D2h, order 8). This geometric symmetry reduction from Pm3¯m to Pmmm may play the role of the spontaneous breaking of the

 doi:10.20944/preprints202604.0893.v1

chiral symmetry group SU(2)L × SU(2)R → SU(2)V that characterizes the QCD vacuum. According to Goldstone's theorem, each continuously broken symmetry generator produces one massless Goldstone boson. The three broken rotational directions of the cube, the three independent ways of rotating between x, y, and z that are no longer symmetries of the Pmmm space group, correspond to three independent broken generators, producing three Goldstone bosons identified as the pions π^+, π^-, and π^0. The multiplicity-3 of the Wyckoff positions 3c and 3d, which transforms as the T1u irreducible representation of Oh, a polar vector representation, provides the geometric origin of the SU(2) isospin triplet structure of the pion field. The QCD pion triplet is therefore encoded in the geometry of the $Pm\bar{3}m \rightarrow Pmmm$ symmetry reduction at the level of the crystal structure of the proposed chiral condensate vacuum

References

1. Oaknin, D.H and Zhitnitsky, A., (2004), "Baryon Asymmetry, Dark Matter and Quantum Chromodynamics", https://arxiv.org/abs/hep-ph/0309086
2. Brown, F.R., (1990), *"On the existence of a phase transition for QCD with three light quarks,"* Phys. Rev. Lett. **65**, 2491.
3. Aoki, Y., Fodor, Z., Katz, S.D., Szabo, K.K., (2006), "The QCD transition temperature: results with physical masses in the continuum limit",Phys. Lett. B 643, 46, https://arxiv.org/abs/hep-lat/0609068
4. Bazavov, A., et al., (2012), *"Chiral and deconfinement aspects of the QCD transition,"* Phys. Rev. D **85**, 054503, https://arxiv.org/abs/1111.1710
5. Bazavov, A., et al., (2019) *"Chiral crossover in QCD at zero and non-zero chemical potentials,"* Phys. Lett. B **795**, 15, https://arxiv.org/abs/1812.08235
6. DeGrand, T., Schaefer, S., (2005), "Chiral properties of two-flavor QCD in small volume and at large lattice spacing", https://arxiv.org/pdf/hep-lat/0506021
7. Schaefer, T., Shuryak, E., (1999), "Instantons in QCD", https://arxiv.org/pdf/hep-ph/9610451
8. Banks, T., and Casher, A., (1980), "Chiral symmetry breaking in confining theories," Nucl. Phys. B 169, 103.
9. Helge, K., (2009), "Wave Packets, Compendium of Quantum Physics, Concepts, Experiments, History and Philosophy.", 828–830, Springer. https://link.springer.com/chapter/10.1007/978-3-540-70626-7_232
10. Darwin, C. G.,(1927), "Free motion in the wave mechanics", Proceedings of the Royal Society of London. https://royalsocietypublishing.org/doi/10.1098/rspa.1927.0179
11. Dirac, P. A. M., (1956), "Electrons and the Vacuum (lecture)",
12. https://mediatheque.lindau-nobel.org/recordings/31423/electrons-and-the-vacuum-1956#:~:text=A%20bare%20electron%20is%20a,we%20use%20the%20electromagnetic%20potentials.
13. Aharonov, Y., Davidovich, L., & Zagury, N. Quantum random walks. Phys. Rev. A, 48, 1687 (1993).
14. Kempe, J., (2005), "Quantum random walks—an introductory overview", https://arxiv.org/abs/quant-ph/0303081
15. Lovett, N. B., Cooper, S., Everitt, M., Trevers, M., and Kendon, V., (2010), "Universal quantum computation using the discrete time quantum walk", https://arxiv.org/abs/0910.1024
16. [15] Kitagawa, T., Rudner, M., Berg, E., and Demler, E., (2010), "Exploring Topological Phases With Quantum Walks", https://arxiv.org/abs/1003.1729.
17. Nemirovsky-Levy, L., Lyubarov, M., Plotnik, Y., Segal, O., Segev, M., (2024), "Topological Protection of Bell States in a Two-Dimensional Quantum Walk", https://opg.optica.org/viewmedia.cfm?uri=CLEO_FS-2024-FW3M.4&seq=0
18. Perets, H.B., Lahini, Y., Pozzi, F., Sorel, M., Morandotti, R., Silberberg, Y., "Realization of quantum walks with negligible decoherence in waveguide lattices", https://arxiv.org/abs/0707.0741
19. Melnikov, A., Fedichkin, L.E., (2016),"Quantum walks of interacting fermions on a cycle graph", https://www.nature.com/articles/srep34226
20. Williams, S., Malik, S., Spannowsky, M., Bepari, K., (2022), "Quantum walk approach to simulating Parton showers", https://arxiv.org/abs/2109.13975
21. Brodsky, S. B., Roberts, C. D., Shrock, R., Tandy, P.C., (2010), "Essence of the vacuum quark condensate", https://arxiv.org/abs/1005.4610

 doi:10.20944/preprints202604.0893.v1

22. Corley, S., Jacobson, T., "Black Hole Lasers", (1999), https://arxiv.org/pdf/hep-th/9806203.pdf
23. Hawking, S., (1975), "Particle Creation by Black Holes", Commun. math. Phys. 43, 199-220, https://www.brainmaster.com/software/pubs/physics/Hawking%20Particle%20Creation.pdf
24. Rom, R., (2023), "Matter Reactors", Journal of High Energy Physics, Gravitation and Cosmology, 9, No. 2. https://www.scirp.org/journal/paperinformation.aspx?paperid=124154
25. Rom, R., (2025), "Behind and Beyond the Standard Model",
26. https://www.scirp.org/journal/paperinforcitation?paperid=144430
27. Harari, H., (1979), "A Schematic Model of Quarks and Leptons", https://www.weizmann.ac.il/particle/harari/sites/particle.harari/files/uploads/schematic_model_of_quarks_and_leptons.pdf
28. Heisenberg, W., (1933), "The development of quantum mechanics", Nobel Lecture,
29. https://www.nobelprize.org/uploads/2018/06/heisenberg-lecture.pdf
30. Einstein, A., (2016), "The Foundation of the General Theory of Relativity",
31. https://isidore.co/misc/Physics%20papers%20and%20books/St.%20John's%20College's,%20TAC's%20curricula's,%20et%20alii%20sci.%20papers/1916-%20The%20Foundation%20of%20the%20General%20Theory%20of%20Relativity%20(Einstein).pdf
32. Dirac, P.A.M., (1926), "On the Theory of Quantum Mechanics", https://royalsocietypublishing.org/doi/pdf/10.1098/rspa.1926.0133

33. Even, J. et al., "Symmetry-Based Tight Binding Modeling of Halide Perovskites," *Journal of Physical Chemistry Letters*, 2016.
34. Blinder, S. M., (2018), "Ammonia Inversion Energy Levels using Operator Algebra", https://arxiv.org/abs/1809.08178.
35. Rom, R., (Apr 2023), "The Quantum Chromodynamics Gas Density Drop and the General Theory of Relativity Ether", Journal of High Energy Physics, Gravitation and Cosmology,
36. 9, No. 2. https://www.scirp.org/journal/paperinformation.aspx?paperid=124153
37. Bardeen, J., Cooper, L.N., Schrieffer, J.R., (1957), "Theory of Superconductivity", Phys.
38. Rev. 108, 1175, https://journals.aps.org/pr/pdf/10.1103/PhysRev.108.1175
39. Balatsky, A.V, Roushan, P., Schaltegger, J. and. Wong, P.J., (2024),"Quantum Sensing from Gravity as Universal Dephasing Channel for Qubits", https://arxiv.org/abs/2406.03256
40. Seigel, H.O., (1999), "A GUIDE TO HIGH PRECISION LAND GRAVIMETER SURVEYS",
41. https://scintrexltd.com/wp-content/uploads/2017/02/Guide-High-Precision-Land-Gravimeter-Surveys.pdf
42. Bocchieri, P. & Loinger, A., (1957), "Quantum recurrence theorem", Phys. Rev. 107, 337.
43. Wallace, D., (2015), "Recurrence theorems: a unified account.", J. Math. Phys. 56, 022105.
44. Davidson, A., (2024),"Are Leptons as elementary as Quarks?", https://arxiv.org/pdf/2210.16177
45. Zhang, Q., Wu, B., (2025), "Physics and Computation: A Perspective From Non-Hermitian Quantum Computer", https://arxiv.org/pdf/2506.18012
46. Alice Collaboration, (2025), "Revealing the microscopic mechanism of deuteron formation at the LHC", https://arxiv.org/abs/2504.02393
47. Bloch. F., (1929), "The Quantum Mechanics of Electrons in Crystal Lattices", http://courses.physics.ucsd.edu/2018/Fall/physics211a/topic/bloch.pdf